1975

Stabilization System Environmental Disturbance Modeling and Analysis

Lawrence E. Sieb
University of Central Florida, larry@medtechcon.com

STABILIZATION SYSTEM ENVIRONMENTAL DISTURBANCE MODELING AND ANALYSIS

BY

LAWRENCE E. SIEB, JR.
B.S. Michigan State University, 1969

THESIS

Submitted in partial fulfillment of the requirements
for the degree of Master of Science in Engineering
in the Graduate Studies Program of
Florida Technological University

Orlando, Florida
1975

TABLE OF CONTENTS

LIST OF FIGURES

1.0 INTRODUCTION

Systems that operate in airborne environments and rely on the resolution provided by optical sensors require a stabilization system to isolate the line-of-sight (LOS) from the operating environment. For systems employing television sensors, stabilization accuracy is of prime importance in maintaining sufficient picture resolution to allow target identification and recognition at maximum ranges. The development of system models that accurately predict stabilization performance is important both in design trade offs and in the system design and testing [1].

Two basic concepts are available for achieving LOS stabilization; momentum stabilization which employs a spinning mass and rate stabilization which utilizes inertial rate sensors. Previously rate stabilized platforms have been employed for high performance laser designator systems mounted in aircraft while momentum stabilized platforms have been used on tactical missiles. Rate stabilized platforms have not been used often in tactical missiles due to their higher cost and the lack of high performance stabilization requirements over large field-of-regards on the missile seekers. Currently, more TV sensors are being proposed for

tactical missiles with long stand off range requirements, hence higher LOS stabilization performance. New inertial rate sensors are also being developed which promise to significantly lower the production cost of rate stabilized platforms. The relative performance capability inherent in the two types of systems has not yet been rigorously treated. This subject is of interest now due to the increasing importance of LOS stabilization in missile seekers and the cost/performance trade studies that must be performed to select the more optimal of the two stabilization concepts for a particular application.

This paper develops the system models necessary to evaluate the LOS stabilization performance for either concept. These models are presented in detail for each concept to provide an understanding of the basic physical phenomena which determines the LOS stabilization performance achievable with each concept. Since the basic LOS stabilization models are developed in a linear fashion, the extension to the nonlinear case is also included as are techniques for determining system performance. To demonstrate the validity of the models derived, a case study is presented covering both momentum and rate stabilized systems which is verified with simulation results. The primary value of this paper lies in the model derivation and the detailed presentation of these models which provides insight into the relationship of the system parameters with the techniques necessary to predict

LOS stabilization performance for both rate and momentum stabilized platforms.

2.0 THEORY

2.1 Stabilization System Description

The two basic concepts available for achieving LOS stabilization are momentum stabilization and rate stabilization. Generally, both systems can be implemented with a two-degree-of-freedom gimbal platform which provides LOS stabilization about the two axes orthogonal to the LOS. Momentum stabilization is accomplished through the use of a large spinning wheel supported in two gimbals. Since the angular momentum vector possessed by the spinning wheel tends to remain fixed in inertial space unless external torques are applied, LOS stabilization is achieved. A rate stabilized platform utilizes two rate (or rate integrating) gyros mounted on the inner gimbal with their input axes orthogonal to the LOS to stabilize the LOS in inertial space. The primary control problem is not that of commanding the platform LOS but rather that of minimizing the LOS motion induced by undesired torques. This paper, then, is concerned with deriving the models necessary to demonstrate the effect of the system parameters on the degree of LOS isolation achieved.

A two-degree-of-freedom gimbal platform will represent a general case for either system. A sketch of an outer pitch, inner yaw gimbal platform is presented in Figure 1. A separate, orthogonal set of coordinates are associated with both the inner and outer gimbals, the base, and inertial space. These are identified with the subscripts IG, OG, B, and I respectively. Subscripts will be used to identify the measured parameter and reference frame, i.e., $\Psi_{IG/OG}$ refers to the inner gimbal yaw angle measured relative to the outer gimbal reference frame. Zero relative gimbal angles are defined as occurring when x_{IG}, x_{OG}, x_B are coincident.

The gimbal sketch is general in that it applies to either stabilization method defined earlier as does the primary disturbance source which is the aircraft environment. More specifically, the components of linear vibration (acceleration) orthogonal to the gimbal rotational axes couple into LOS motion through the appropriate gimbal mass unbalance, while angular vibration couples into LOS motion through the friction and compliance associated with each gimbal. Thus, the two most significant performance indices for a LOS stabilization system are the torque disturbance rejection (TDR) ratio and the angular disturbance (ADR) ratio. The TDR ratio is defined as the ratio of LOS motion to torque disturbance and the ADR ratio is defined as the ratio of LOS motion to the angular rate of an adjacent gimbal.

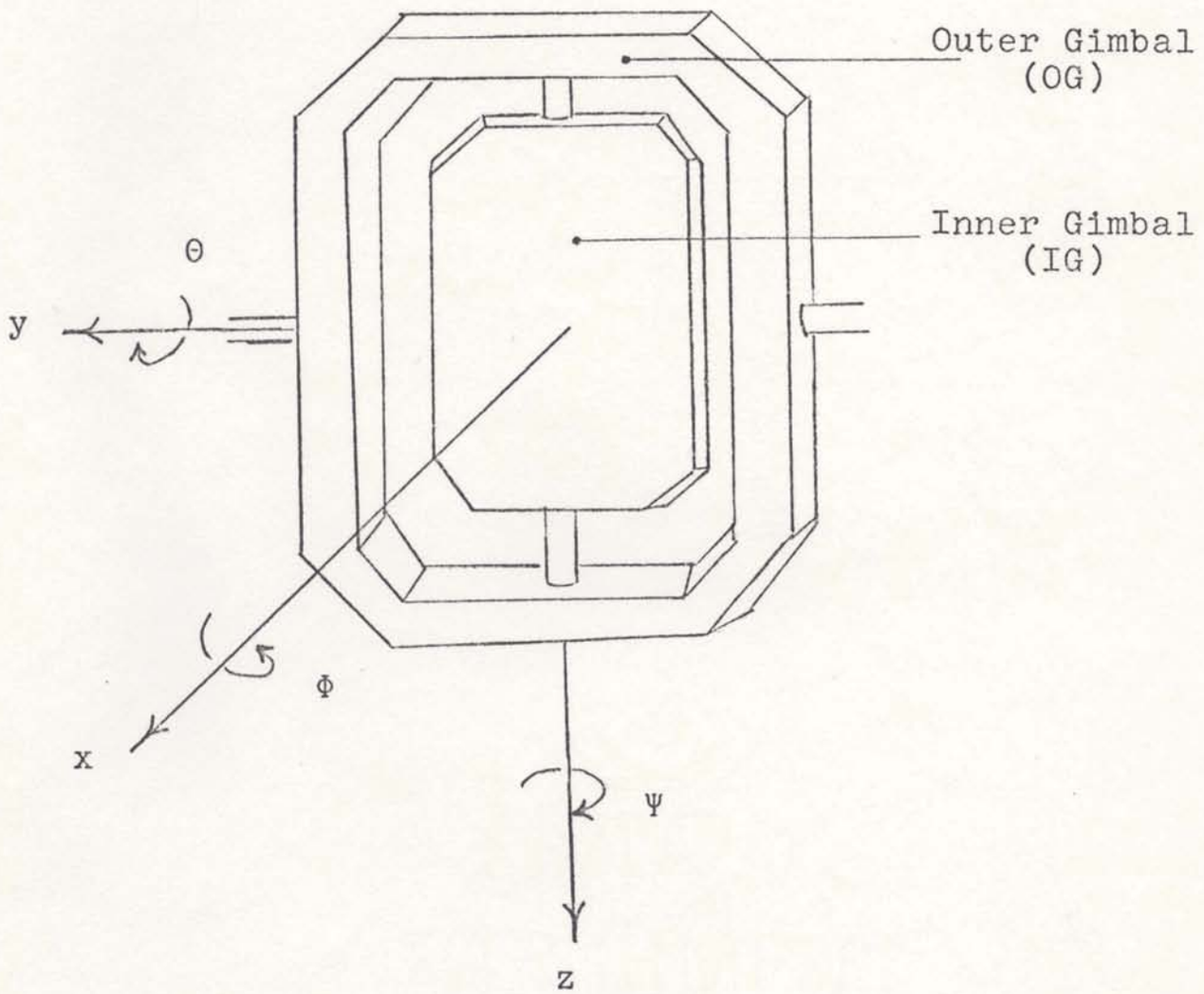

Figure 1. 2-DOF Gimbal Platform

2.2 System Equations and Solution

The dynamic equations are fully derived in Appendix 5.1 from Newton's second law for angular motion. These equations represent the general case for LOS stabilized platforms since the defining system equations for rate stabilized systems may be derived from the momentum solution by setting the angular momentum term equal to zero and adding an additional damping term to include the effects of rate gyro feedback.

From Appendix 5.1, the defining equations for a momentum stabilized platform including the linear and angular environments are:

$$\Sigma T_{IG} = J_I \ddot{\Psi}_{\underset{I}{IG}} - H\dot{\Theta}_{\underset{I}{IG}} = - K_{WI} \Psi_{\underset{OG}{IG}} - F_I \left(\dot{\Psi}_{\underset{I}{IG}} - \dot{\Psi}_{\underset{I}{OG}}\right) + T_{DI}$$

$$\Sigma T_{OG} = J_O \ddot{\Theta}_{\underset{I}{OG}} + H \left(\cos \Psi_{\underset{OG}{IG}}\right) \dot{\Psi}_{\underset{I}{IG}} \qquad (1)$$

$$= - K_{WO} \Theta_{\underset{B}{OG}} - F_O \left(\dot{\Theta}_{\underset{I}{OG}} - \dot{\Theta}_{\underset{I}{B}}\right) + T_{DO}$$

where:

ΣT_{IG} = sum of the external torques about the inner gimbal rotational axis

ΣT_{OG} = sum of the external torques about the outer gimbal rotational axis

J_I/J_O = inner/outer gimbal inertias about their respective rotational axis

F_I/F_O = inner/outer gimbal friction coefficient

K_{WI}/K_{WO} = inner/outer gimbal spring constant

T_{DI}/T_{DO} = inner/outer gimbal mass unbalance torques

H = angular momentum of spinning wheel

and all angular motion terms conform to the notation previously defined. These equations are represented in block diagram form in Figure 2.

The system equations may be more conveniently expressed using state notation employing the following definitions:

$$\begin{bmatrix} X_1 \\ X_2 \\ X_3 \\ X_4 \end{bmatrix} = \begin{bmatrix} \dot{\Psi}_{IG/I} \\ \dot{\Theta}_{OG/I} \\ \Psi_{IG/OG} \\ \Theta_{OG/B} \end{bmatrix}; \quad \begin{bmatrix} y_1 \\ y_2 \end{bmatrix} = \begin{bmatrix} \dot{\Psi}_{IG/I} \\ \dot{\Theta}_{IG/I} \end{bmatrix}; \quad \begin{bmatrix} U_1 \\ U_2 \\ U_3 \\ U_4 \\ U_5 \end{bmatrix} = \begin{bmatrix} T_{DI} \\ T_{DO} \\ \dot{\Psi}_{OG/I} \\ \dot{\Theta}_{B/I} \\ \dot{\Phi}_{OG/I} \end{bmatrix}$$

The angular disturbance rate inputs are formed from the body rates using Euler transformation as:

$$\begin{bmatrix} \dot{\Phi}_{OG/I} \\ \dot{\Theta}_{OG/I} \\ \dot{\Psi}_{OG/I} \end{bmatrix} = \left[\Theta_{OG/B}\right] \begin{bmatrix} \dot{\Phi}_{B/I} \\ \dot{\Theta}_{B/I} \\ \dot{\Psi}_{B/I} \end{bmatrix}; \quad \begin{bmatrix} \dot{\Phi}_{IG/I} \\ \dot{\Theta}_{IG/I} \\ \dot{\Psi}_{IG/I} \end{bmatrix} = \left[\Psi_{IG/OG}\right] \begin{bmatrix} \dot{\Phi}_{OG/I} \\ \dot{\Theta}_{OG/I} \\ \dot{\Psi}_{OG/I} \end{bmatrix}$$

where $\left[\Theta_{OG/B}\right]$ and $\left[\Psi_{IG/OG}\right]$ are the Euler pitch and yaw transformations:

$$\left[\Theta_{OG/B}\right] = \begin{bmatrix} \cos\Theta_{OG/B} & 0 & -\sin\Theta_{OG/B} \\ 0 & 1 & 0 \\ \sin\Theta_{OG/B} & 0 & \cos\Theta_{OG/B} \end{bmatrix}$$

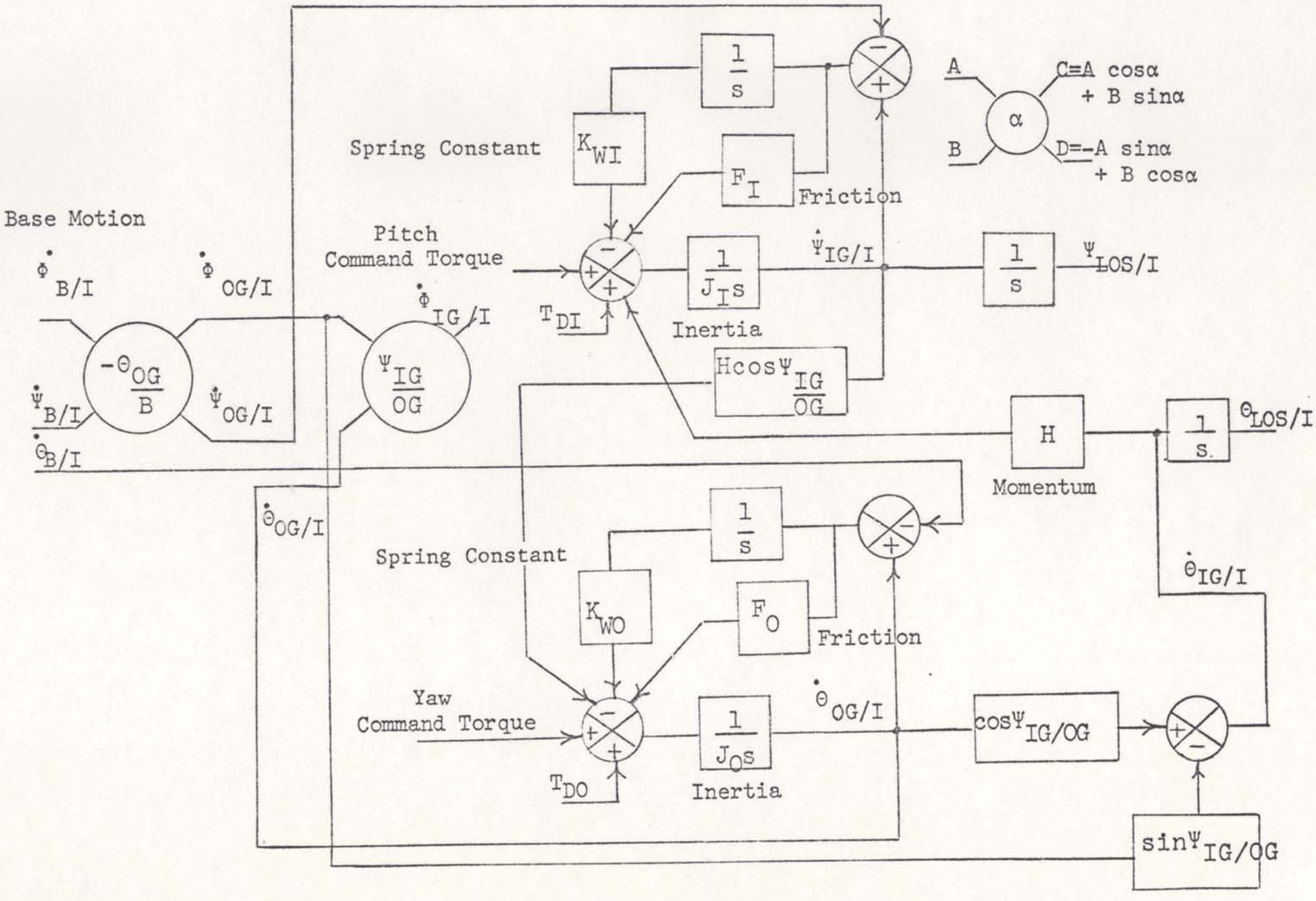

Figure 2. Momentum Stabilized Platform Block Diagram

$$\left[\Psi_{IG/OG}\right] = \begin{bmatrix} \cos\Psi_{IG/OG} & \sin\Psi_{IG/OG} & 0 \\ -\sin\Psi_{IG/OG} & \cos\Psi_{IG/OG} & 0 \\ 0 & 0 & 1 \end{bmatrix}$$

Then the defining stabilization equations may be written in the conventional format:

$$\dot{\bar{x}}(t) = [A]\bar{x}(t) + [B]\bar{u}(t)$$

$$\bar{y}(t) = [C]\bar{x}(t) + [D]\bar{u}(t)$$

as,

$$\begin{bmatrix} \dot{x}_1(t) \\ \dot{x}_2(t) \\ \dot{x}_3(t) \\ \dot{x}_4(t) \end{bmatrix} = \begin{bmatrix} -F_I/J_I & H/J_I\cos\Psi_{IG/OG} & -K_{WI}/J_I & 0 \\ -H/J_O\cos\Psi_{IG/OG} & -F_O/J_O & 0 & -K_{WO}/J_O \\ 1 & 0 & 0 & 0 \\ 0 & 1 & 0 & 0 \end{bmatrix} \begin{bmatrix} x_1(t) \\ x_2(t) \\ x_3(t) \\ x_4(t) \end{bmatrix}$$

$$+ \begin{bmatrix} 1/J_I & 0 & F_I/J_I & 0 & -H/J_I\sin\Psi_{IG/OG} \\ 0 & 1/J_O & 0 & F_O/J_O & 0 \\ 0 & 0 & -1 & 0 & 0 \\ 0 & 0 & 0 & -1 & 0 \end{bmatrix} \begin{bmatrix} T_{DI} \\ T_{DO} \\ \dot{\Psi}_{OG/I} \\ \dot{\Theta}_{B/I} \\ \dot{\Phi}_{OG/I} \end{bmatrix}$$

$$\begin{bmatrix} y_1 \\ y_2 \end{bmatrix} = \begin{bmatrix} 1 & 0 & 0 & 0 & 0 \\ 0 & \cos\Psi_{IG/OG} & 0 & 0 & 0 \end{bmatrix} \begin{bmatrix} x_1 \\ x_2 \\ x_3 \\ x_4 \end{bmatrix} +$$

$$\begin{bmatrix} 0 & 0 & 0 & 0 & 0 \\ 0 & 0 & 0 & 0 & -\sin\Psi_{IG/OG} \end{bmatrix} \begin{bmatrix} T_{DI} \\ T_{DO} \\ \dot{\Psi}_{OG/I} \\ \dot{\Theta}_{B/I} \\ \dot{\Phi}_{OG/I} \end{bmatrix}$$

These equations have been solved by calculating the resolvent matrix ($[\Phi(s)]$) and assuming zero initial conditions which yield a solution in the frequency domain of the form:

$$\bar{x}(s) = [\Phi(s)][B]\bar{u}(s) = (s[I]-[A])^{-1}[B]u(s)$$

That is,

$$[x] = \frac{1}{|s[I]-[A]|} \begin{bmatrix} [(s-e)s^2-fs]/J_I & bs^2/J_O \\ ds^2/J_I & [(s-a)s^2 - cs]/J_O \\ [s(s-e)-f]/J_I & bs/J_O \\ ds/J_I & [(s-a)\ s - c\ ]/J_O \end{bmatrix}$$

$$\begin{bmatrix} [(s-e)s^2-fs]\ F_I/J_I - [cs(s-e) - fc] \\ ds^2F_I/J_I - cds \\ [\ s(s-e) - f\ ]F_I/J_I - [(s-a)(s^2-es-f) - bds\ ] \\ ds\ F_I/J_I - cd \end{bmatrix}$$

$$\begin{bmatrix} bs^2\ F_O/J_O - bfs \\ [(s-a)s^2-cs]\ F_O/J_O - (s-a)\ fs + cf \\ bs\ F_O/J_O - bf \\ [s(s-a) - c]F_O/J_O - [(s-a)(s-e)s+ bds + c\ (s-e)\ ] \end{bmatrix}$$

$$\begin{bmatrix} -[(s-e)s^2 - fs]H/J_I \sin\Psi_{IG/OG} \\ -ds^2 H/J_I \sin\Psi_{IG/OG} \\ -[s(s-e) - f]H/J_I \sin\Psi_{IG/OG} \\ -dsH/J_I \sin\Psi_{IG/OG} \end{bmatrix} [u] \qquad (2)$$

where:

$$|s[I]-[A]| = s^4 + (- e - a)s^3 + (ae - f - bd - c)s^2 + (af + ce)s + cf$$

$a = - F_I/J_I$ $\qquad$ $d = (- H/J_O)\cos\Psi_{IG/OG}$

$b = (H/J_I)\cos\Psi_{IG/OG}$ $\qquad$ $e = - F_O/J_O$

$c = - K_{WI}/J_I$ $\qquad$ $f = - K_{WO}/J_O$

The above solution defines the total disturbance rejection performance for momentum stabilized systems. Setting the momentum term equal to zero defines the inherent stabilization achievable with a rate stabilized system but does not include the effects of the electronic compensation involved. The effects of the rate stabilized system servo loop will be included later and shown to establish LOS stabilization performance within the bandwidth of the closed rate gyro loops.

2.3 Momentum Stabilized Platform Disturbance Model

As will be discussed later, stabilization performance is generally evaluated in the frequency domain. To obtain an understanding of the parameters affecting the disturbance rejection responses, the disturbance inputs will be treated

individually.

From the general model solution (equation 2), the torque disturbance rejection response (TDR) of the yaw axis to inner gimbal mass unbalance torques is:

$$\frac{\Psi_{LOS/I}}{T_{DI}}(s) = \frac{1/K_{WI}\left(\frac{J_O}{K_{WO}}s^2 + \frac{F_O}{K_{WO}}s + 1\right)}{\left(\frac{J_O}{K_{WO}}s^2 + \frac{F_O}{K_{WO}}s + 1\right)\left(\frac{J_I}{K_{WI}}s^2 + \frac{F_I}{K_{WI}}s + 1\right) + \frac{H^2}{K_{WO}K_{WI}}\left(\cos^2 \frac{\Psi_{IG}}{OG}\right)s^2} \qquad (3)$$

which may be plotted as shown in the following sketch. The low frequency region approaching zero has not been represented, because it is not generally of interest in determining stabilization jitter. Also, the cosine term in the above transfer function is treated as a constant in the following discussion in order to linearize the results and is usually set to unity except in the cases where it has a significant impact on the results.

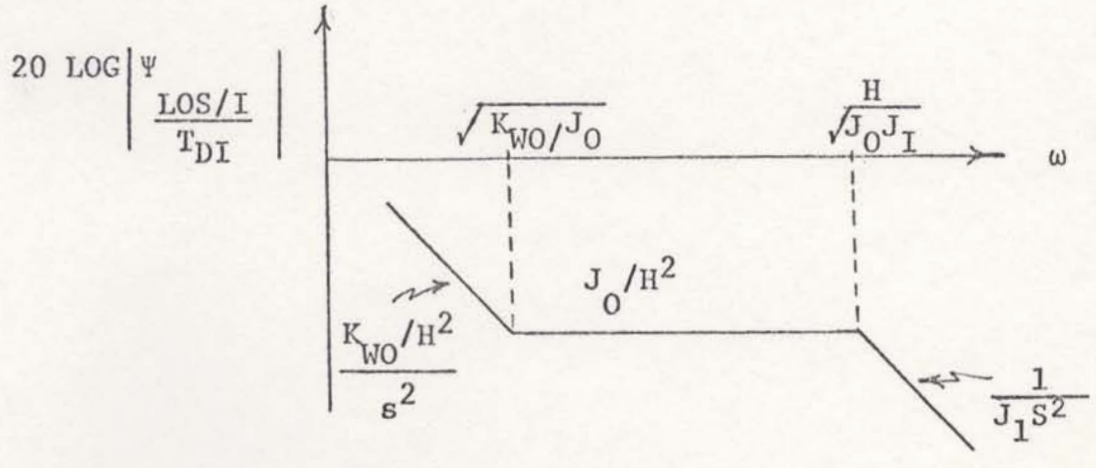

As may be noted from the sketch, the disturbance rejection capability of the yaw axis to inner gimbal mass unbalance torques is determined by different gimbal parameters depending on which of these frequency regions the disturbance occurs within. For real frequencies, $\omega(s=j\omega)$, less than the spring constant-inertia break of the outer gimbal, the TDR response is given by $\frac{\Psi_{LOS/I}}{T_{DI}} = \frac{K_{WO}/H^2}{s^2}$; $\omega < \sqrt{\frac{K_{WO}}{J_O}}$ and, for ω greater than the wire torque-inertia break of the outer gimbal and less than the loop bandwidth,

$$\frac{\Psi_{LOS/I}}{T_{DI}} = \frac{J_O}{H^2} \; ; \; \sqrt{\frac{K_{WO}}{J_O}} < \omega < \frac{H}{\sqrt{J_O J_O}}$$

For frequencies outside the loop bandwidth,

$$\frac{\Psi_{LOS/I}}{T_{DI}} = \frac{1}{J_I s^2} \; ; \quad \omega > H/\sqrt{J_I J_O}$$

These same results may be obtained from the original TDR transfer function with appropriate small and large frequency approximations. For example, at small frequencies, the angular momentum term in the denominator is dominant, so,

$$\frac{\Psi_{LOS/I}}{T_{DI}} = \frac{K_{WO}/H^2 \left(\frac{J_O}{K_{WO}} s^2 + \frac{F_O}{K_{WO}} s + 1\right)}{s^2}; \; \omega < 2\sqrt{\frac{K_{WO}}{J_O}}$$

and for mid-range frequencies, the s^2 term is dominant in the numerator and the s^4, s^3, and $H^2 s^2$ terms predominant in

the denominator yielding,

$$\frac{\Psi_{LOS/I}}{T_{DI}} = \frac{J_O/H^2}{\frac{J_I J_O}{H^2} s^2 + \frac{(J_I F_O + J_O F)}{H^2} s + 1}; \quad \omega > 2\sqrt{\frac{K_{WO}}{J_O}}$$

which with increasing ω, reduces to

$$\frac{\Psi_{LOS/I}}{T_{DI}} = \frac{1}{J_I s^2}; \quad \omega > \frac{H}{\sqrt{J_I J_O}}$$

Thus, within the loop bandwidth the degree of stabilization is primarily determined by the square of the angular momentum, while outside the loop bandwidth, the disturbance rejection is wholly determined by the gimbal inertia. The roll off point of the loop, that is, the system bandwidth, is equal to the momentum over the square root of the product of the gimbal inertias. This is also referred to as the nutation frequency of a momentum stabilized system.

The pitch axis of the LOS responds to the inner gimbal mass unbalance torques with the following TDR as reduced from the general solution of equation (2).

$$\frac{\Theta_{LOS/I}}{T_{DI}} = \frac{-\cos\Psi_{IG/OG} H/K_{WI}K_{WO} s}{\left(\frac{J_O}{K_{WO}} s^2 + \frac{F_O}{K_{WO}} s + 1\right)\left(\frac{J_I}{K_{WI}} s^2 + \frac{F_I}{K_{WI}} s + 1\right) + \frac{H^2}{K_{WI}K_{WO}} \cos^2\Psi_{\frac{IG}{OG}} s^2} \tag{4}$$

Which plotted as a function of frequency gives:

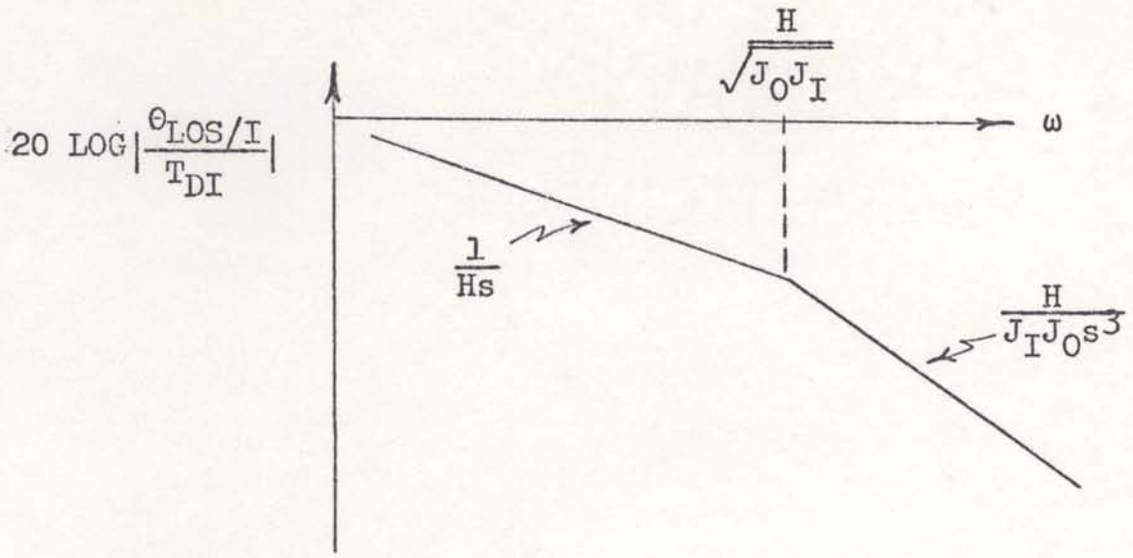

The small and large frequency approximation may be made with the same assumptions used for the inner gimbal TDR.

$$\frac{\Theta_{LOS/I}}{T_{DI}} = -\frac{1/H}{s} \; ; \quad \omega < \frac{H}{\sqrt{J_I J_O}}$$

$$\frac{\Theta_{LOS/I}}{T_{DI}} = \frac{-1/H}{s\left(\frac{J_I J_O}{H^2}s^2 + \frac{(J_I F_O + J_O F_I)}{H^2}s + 1\right)} \; ; \quad \omega > \frac{H}{\sqrt{J_I J_O}}$$

The pitch axis disturbance rejection to inner gimbal mass unbalance torques is determined primarily by the angular momentum term. It should be noted that the inner gimbal has poor dc torque disturbance rejection.

Since the model is symmetrical, the yaw and pitch TDR responses to outer gimbal mass unbalance torques are the same as the pitch and yaw gimbal responses to inner gimbal mass unbalance torques with appropriate parameter changes. These responses are written as follows from the general model:

$$\frac{\Theta_{LOS/I}}{T_{DO}} = \frac{\cos\Psi_{\frac{IG}{OG}}/K_{WO}\left(\frac{J_I}{K_{WI}}s^2 + \frac{F_I}{K_{WI}}s + 1\right)}{\left(\frac{J_O}{K_{WO}}s^2 + \frac{F_O}{K_{WO}}s + 1\right)\left(\frac{J_I}{K_{WO}}s^2 + \frac{F_I}{K_{WI}}s + 1\right) + \frac{H^2}{K_{WO}K_{WI}}\cos^2\Psi_{\frac{IG}{OG}}s^2} \tag{5}$$

$$\frac{\Psi_{LOS/I}}{T_{DO}} = \frac{(H\cos\Psi_{IG/OG}/K_{WI}K_{WO})\,s}{\left(\frac{J_O}{K_{WO}}s^2 + \frac{F_O}{K_{WO}}s + 1\right)\left(\frac{J_I}{K_{WI}}s^2 + \frac{F_I}{K_{WI}}s + 1\right) + \frac{H^2}{K_{WO}K_{WI}}\cos^2\Psi_{\frac{IG}{OG}}s^2}$$

The related sketches and low frequency approximations made for the inner gimbal mass unbalance torques also apply to the outer gimbal mass unbalance TDR responses.

The yaw angular disturbance rejection response (ADRy) determines the amount of LOS motion due to body induced angular rates about the inner gimbal rotational axis. The inner gimbal ADRy response may be reduced from the general model as,

$$\frac{\Psi_{LOS/I}}{\dot{\Psi}_{OG/I}} = \frac{\left(\frac{J_O}{K_{WO}}s^2 + \frac{F_O}{K_{WO}}s + 1\right)\left(\frac{F_I}{K_{WI}}s + 1\right)}{s\left[\left(\frac{J_O}{K_{WO}}s^2 + \frac{F_O}{K_{WO}}s + 1\right)\left(\frac{J_I}{K_{WI}}s^2 + \frac{F_I}{K_{WI}}s + 1\right) + \frac{H^2}{K_{WI}K_{WO}}\cos^2\Psi_{\frac{IG}{OG}}s^2\right]} \tag{6}$$

which may be plotted as,

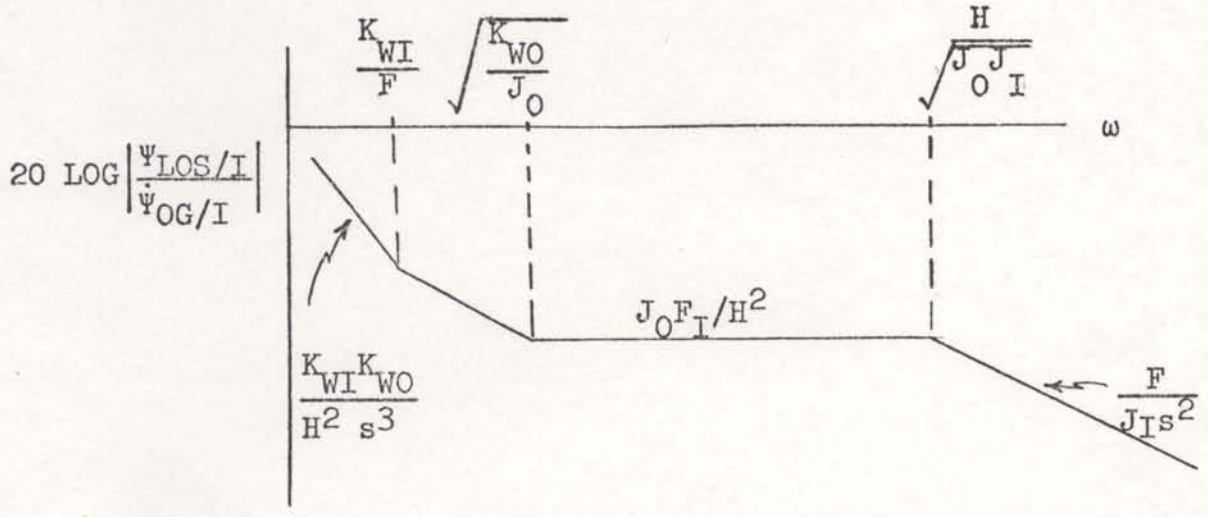

The same assumptions employed to obtain the low and high frequency approximations of the TDR responses may also be used here. That is, at low frequencies the momentum squared term in the denominator may be considered the dominate term and at higher frequencies, the fourth-order, third-order, and second-order s terms in the denominator are the significant terms along with the third-order term in the numerator. These assumptions yield the following approximations from which the ADRy sketch was plotted.

$$\frac{\Psi_{LOS/I}}{\dot{\Psi}_{OG/I}} = \frac{\left(\frac{J_O}{K_{WO}} s^2 + \frac{F_O}{K_{WO}} s + 1\right)\left(\frac{F_I}{K_{WI}} s + 1\right)}{\frac{H^2}{K_{WI} K_{WO}} s^3}; \quad \omega < \frac{H}{\sqrt{J_I J_O}}$$

$$\frac{\Psi_{LOS/I}}{\dot{\Psi}_{OG/I}} = \frac{\frac{J_O F_I}{H^2}}{\frac{J_I J_O}{H^2} s^2 + \frac{(J_I F_O + J_O F_I)}{H^2} s + 1}; \quad \omega > \frac{H}{\sqrt{J_I J_O}}$$

Thus, the disturbance rejection capability is dependent upon the square of the angular momentum at frequencies within the natural frequency of the gimbal system, while at frequencies greater than this, the rejection is inversely proportional to the inner gimbal inertia. The sketch also shows that the angular disturbance couples through the spring constant at low frequencies and through the gimbal friction at higher frequencies.

The pitch axis response to yaw (inner) gimbal angular disturbance inputs may be written from the general solution as:

$$\frac{\Theta_{LOS/I}}{\dot{\Psi}_{OG/I}} = \frac{-\frac{H}{K_{WO}}\cos^2\Psi\frac{IG}{OG}\left(\frac{F_I}{K_{WI}}s + 1\right)}{\left(\frac{J_O}{K_{WO}}s^2 + \frac{F_O}{K_{WO}}s + 1\right)\left(\frac{J_I}{K_{WI}}s^2 + \frac{F_I}{K_{WI}}s + 1\right) + \frac{H^2}{K_{WI}K_{WO}}\cos^2\Psi\frac{IG}{OG}s^2} \qquad (7)$$

and sketched as a function of ω.

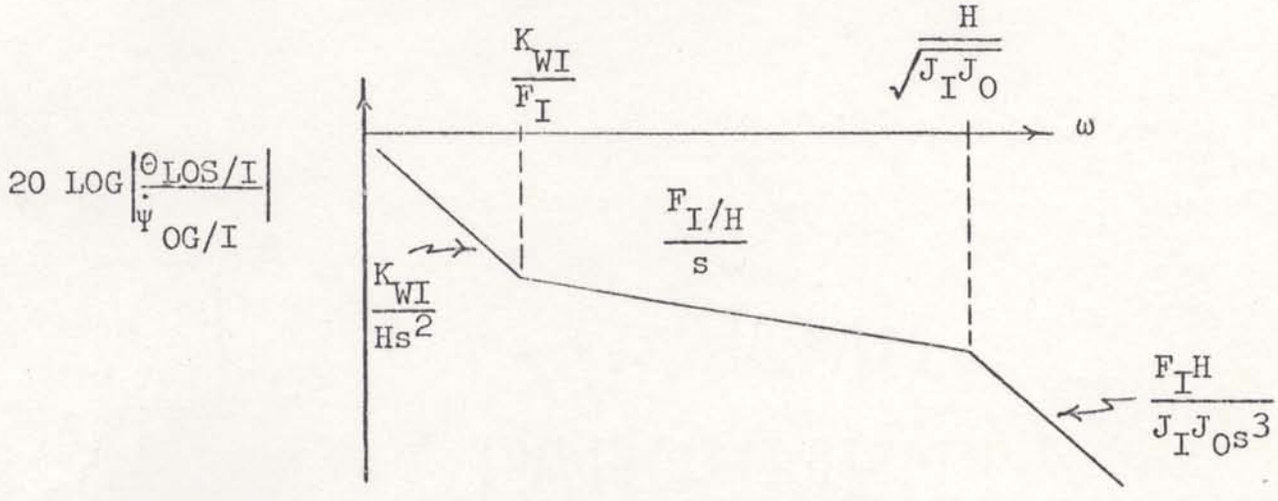

Utilizing the low and high frequency approximations used for the yaw axis ADR approximations, the pitch axis ADR may be represented from equation (7) as:

$$\frac{\Theta_{LOS/I}}{\dot{\Psi}_{OG/I}} = \frac{-K_{WI}\left(\frac{F_I}{K_{WI}}s + 1\right)}{Hs^2} \quad ; \quad \omega < \frac{H}{\sqrt{J_I J_O}}$$

$$\frac{\Theta_{LOS/I}}{\dot{\Psi}_{OG/I}} = \frac{-F_I/H}{\frac{J_I J_O}{H^2}s^2 + \frac{(J_I F_O + J_O F_I)}{H^2}s + 1} \quad ; \quad \omega > \frac{H}{\sqrt{J_I J_O}}$$

In this case the primary disturbance rejection is provided by the angular momentum. The angular motion is shown to be coupling through the inner gimbal spring constant term at low frequencies, through the inner gimbal friction at the mid-frequency range, and through the angular momentum at high frequencies where it is attenuated by the product of the inertias.

The angular disturbance rejection responses due to body rates about the outer gimbal rotational axis are of the same form as the gimbal system responses to body rates about the inner gimbal yaw axis just presented. These have been reduced from the general solution to be

$$\frac{\Theta_{LOS/I}}{\dot{\Theta}_{B/I}} = \frac{\cos\Psi_{IG/OG}\left(\frac{J_I}{K_{WI}}s^2 + \frac{F_I}{K_{WI}}s + 1\right)\left(\frac{F_O}{K_{WO}}s + 1\right)}{s\left[\left(\frac{J_O}{K_{WO}}s^2 + \frac{F_O}{K_{WO}}s + 1\right)\left(\frac{J_I}{K_{WI}}s^2 + \frac{F_I}{K_{WI}}s + 1\right) + \frac{H^2}{K_{WI}K_{WO}}\cos^2\Psi_{\frac{IG}{OG}}s^2\right]}$$

$$\frac{\Psi_{LOS/I}}{\dot{\Theta}_{B/I}} = \frac{\frac{H\cos\Psi_{IG/OG}}{K_{WI}}\left(\frac{F_O}{K_{WO}}s + 1\right)}{\left(\frac{J_O}{K_{WO}}s^2 + \frac{F_O}{K_{WO}}s + 1\right)\left(\frac{J_I}{K_{WI}}s^2 + \frac{F_I}{K_{WI}}s + 1\right) + \frac{H^2}{K_{WI}K_{WO}}\cos^2\Psi_{\frac{IG}{OG}}s} \quad (8)$$

The sketches and approximate responses derived for the inner gimbal angular disturbance ($\dot{\Psi}_{OG/I}$) also apply here with appropriate parameter changes.

The last primary disturbance input to be considered is roll angular rates of the outer gimbal. The LOS pitch motion induced by this disturbance may be reduced from equation (2) as:

$$\frac{\Theta_{LOS/I}}{\dot{\Phi}_{OG/I}} = \frac{-\sin\Psi_{IG/OG}\left(\frac{J_O}{K_{WO}}s^2 + \frac{F_O}{K_{WO}}s + 1\right)\left(\frac{J_I}{K_{WI}}s^2 + \frac{F_I}{K_{WI}}s + 1\right)}{s\left[\left(\frac{J_O}{K_{WO}}s^2 + \frac{F_O}{K_{WO}}s + 1\right)\left(\frac{J_I}{K_{WI}}s^2 + \frac{F_I}{K_{WI}}s + 1\right) + \frac{H^2}{K_{WI}K_{WO}}\cos\Psi_{\frac{IG}{OG}}s^2\right]} \quad (9)$$

which as a function of frequency is,

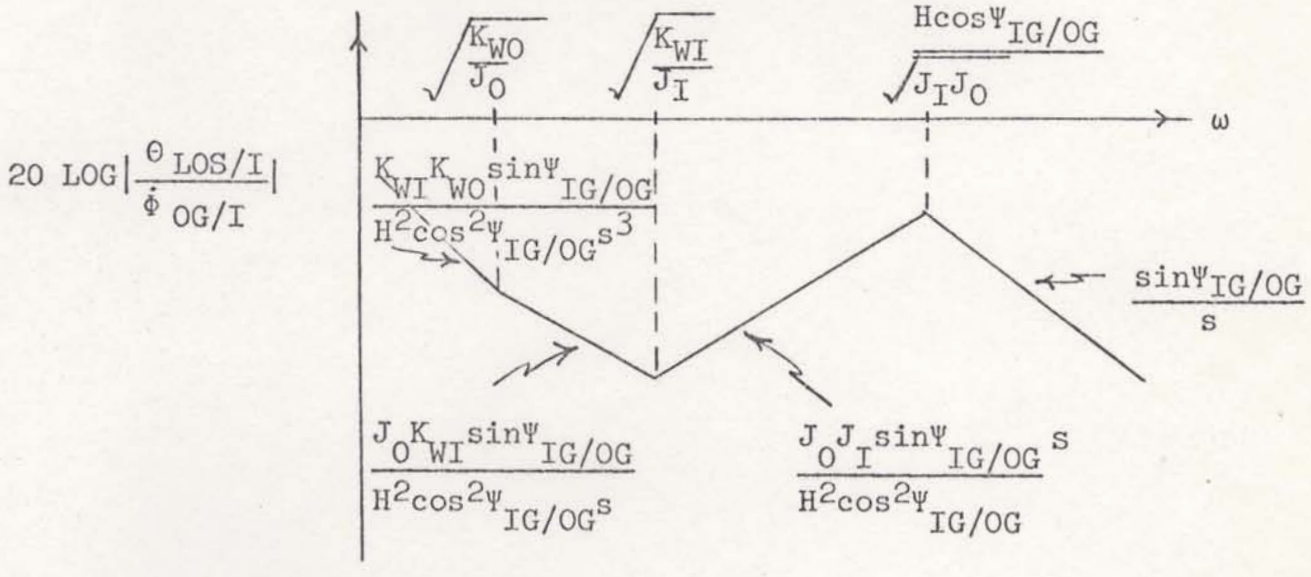

and may be approximated as follows:

$$\frac{\Theta_{LOS/I}}{\dot{\Phi}_{OG/I}} = \frac{-\sin\Psi_{IG/OG}\left(\frac{J_O}{K_{WO}}s^2 + \frac{F_O}{K_{WO}}s + 1\right)\left(\frac{J_I}{K_{WI}}s^2 + \frac{F_I}{K_{WI}}s + 1\right)}{\frac{H^2}{K_{WI}K_{WO}}\cos^2\Psi_{\underline{IG}}s^3} ;$$

$$\omega < \frac{H\cos\Psi_{IG/OG}}{\sqrt{J_I J_O}}$$

$$\frac{\Theta_{LOS/I}}{\dot{\Phi}_{OG/I}} = \frac{-\sin\Psi_{IG/OG}\left(\frac{J_O J_I}{H^2\cos^2\Psi_{IG/OG}}\right)}{\frac{J_I J_O}{H^2\cos^2\Psi_{\underline{IG}}}s^2 + \frac{J_I F_O + J_O F}{H^2\cos^2\Psi_{\underline{IG}}}s + 1} ; \quad \omega > \frac{H\cos\Psi_{IG/OG}}{\sqrt{J_I J_O}}$$

Thus, at frequencies greater than the loop natural frequency, roll motion couples directly into pitch LOS motion through the sine of the inner gimbal angle.

The yaw axis response to outer gimbal roll motion is represented by

$$\frac{\Psi_{LOS/I}}{\dot{\Phi}_{OG/I}} = \frac{-\frac{H\sin\Psi_{IG/OG}}{K_{WI}}\left(\frac{J_O}{K_{WO}}s^2 + \frac{F_O}{K_{WO}}s + 1\right)}{\left(\frac{J_O}{K_{WO}}s^2 + \frac{F_O}{K_{WO}}s + 1\right)\left(\frac{J_I}{K_{WI}}s^2 + \frac{F_I}{K_{WI}}s + 1\right) + \frac{H^2}{K_{WI}K_{WO}}\cos^2\Psi_{\underline{IG}}s^2} \qquad (10)$$

which as a function of frequency looks like,

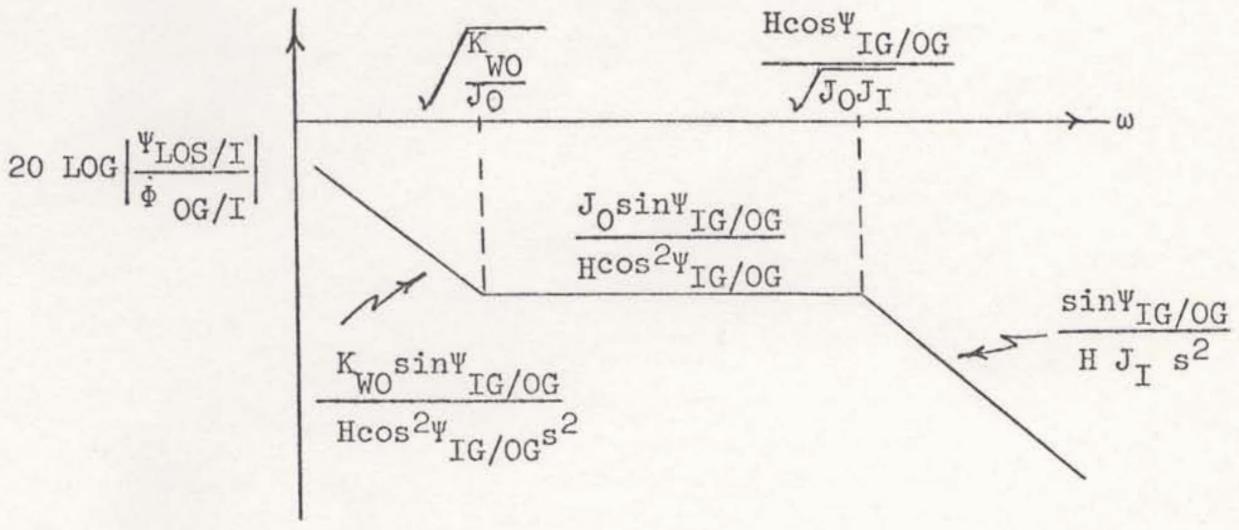

and may be written as

$$\frac{\Psi_{LOS/I}}{\dot{\Phi}_{OG/I}} = \frac{\frac{K_{WO}\sin\Psi_{IG/OG}}{H\cos^2\Psi_{IG/OG}}\left(\frac{J_O}{K_{WO}}s^2 + \frac{F_O}{K_{WO}}s + 1\right)}{s^2}; \quad \omega < \frac{H}{\sqrt{J_I J_O}}$$

$$\frac{\Psi_{LOS/I}}{\dot{\Phi}_{OG/I}} = \frac{\frac{J_O \sin\Psi_{IG/OG}}{H\cos^2\Psi_{IG/OG}}}{\frac{J_I J_O}{H^2\cos^2\Psi_{\frac{IG}{OG}}}s^2 + \frac{J_I F_O + J_O F_I}{H^2\cos\Psi_{\frac{IG}{OG}}}s + 1}; \quad \omega > \frac{H}{\sqrt{J_I J_O}}$$

Then the yaw axis does have more attenuation due to the angular momentum to this particular input than the pitch axis.

2.4 Rate Stabilized Platform Disturbance Models

As mentioned previously, the momentum stabilized platform dynamics define the general case from which the rate stabilization dynamics may be derived by setting the angular momentum term equal to zero. While this does give the solution, considering only the gimbal physical parameters, it does not account for the effects of the loop closed through the rate gyro and associated electronics. An additional term representing this loop must be included in the defining dynamic equations which for the rate stabilized platform (i.e., H=0) become:

$$\Sigma T_{IG} = J_I \ddot{\Psi}_{IG/I} = -K_{WI}\Psi_{IG/OG} - F_I\left(\dot{\Psi}_{IG/I} - \dot{\Psi}_{OG/I}\right) - G_I(s)\dot{\Psi}_{IG/I} + T_{DI} \tag{11}$$

$$\Sigma T_{OG} = J_O \ddot{\Theta}_{OG/I} = -K_{WO}\Theta_{OG/B} - F_O\left(\dot{\Theta}_{OG/I} - \dot{\Theta}_{B/I}\right) - G_O(s)\dot{\Theta}_{IG/I} + T_{DO}$$

where $G_I(s)$ and $G_O(s)$ represent the inner and outer gimbal rate gyros and associated servo compensation as shown in Figure 3. The general solution presented in equation (2) requires the redefinition of 'a' as $a = -(F_I + G_I(s))/J_I$ and 'e' as $e = -(F_O + G_O(s)\cos\Psi_{IG/OG})/J_O$ and the addition of $-G_O(s)(\sin\Psi_{IG/OG})\dot{\Phi}_{OG/I}$ to b_{25} in the general state equation definition. This addition requires adding $-[(s-a)s^2 - cs]\,G_O(s)\sin\Psi_{IG/OG}$ and $-[s(s-a) - c]\,G_O(s)\sin\Psi_{IG/OG}$ to ϕ_{25} and ϕ_{45} respectively in the general solution (2) which along with setting H to zero modifies the solution for rate stabilized platforms.

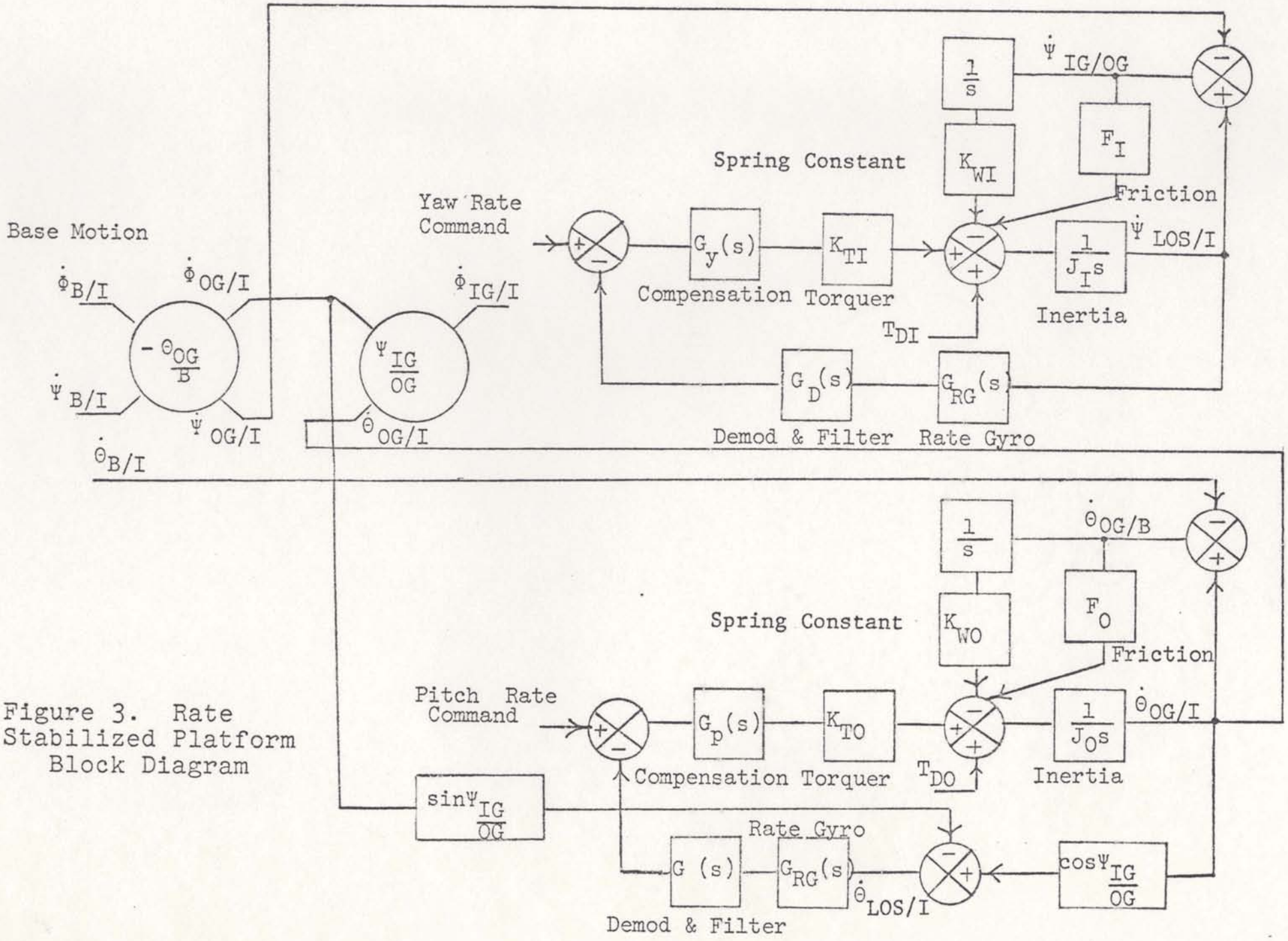

Figure 3. Rate Stabilized Platform Block Diagram

The disturbance rejection solutions will be examined in detail for the rate stabilized platform. In doing this, it is desirable to approximate the rate gyro and servo electronics ($G_I(s)$ and $G_0(s)$ with its most significant parameters. For the following discussion, $G_I(s)$ and $G_0(s)$ will be approximated by $K(1 + s/\omega_n)/s$ where K is the gain term associated with $G_I(s)$ and $G_0(s)$ when written in the normalized form. This is generally valid for the following reasons:

1. Integral compensation is necessary to provide reasonable low frequency disturbance rejection. The associated lead term is required to provide a stable loop and is included for completeness.

2. Any additional shaping within the loop bandwidth is generally done to increase low and mid-frequency gain, that is, employing a lag-lead circuit at these frequencies commonly referred to as an integrating dipole. This additional shaping can be easily incorporated into the solution later.

3. The high frequency poles, due to the rate gyro and any noise filters, have a minimum effect on the disturbance rejection responses.

4. Any lead shaping after the loop bandwidth affects the amount of closed loop peaking which is not being considered in this type solution.

Modifying equation (2) to reflect the special case of a rate stabilized platform, the yaw axis TDR is reduced as

$$\frac{\Psi_{LOS/I}}{T_{DI}} = \frac{1/K_{WI}}{\frac{J_I}{K_{WI}}s^2 + \frac{F_I + G_I(s)}{K_{WI}}s + 1} \qquad (12)$$

Substituting $G(s) = K(1 + s/\omega_n)/s$, gives

$$\frac{\Psi_{LOS/I}}{T_{DI}} = \frac{1/(K + K_{WI})}{\frac{J_I}{K + K_{WI}}s^2 + \frac{F_I + K/\omega_n}{K + K_{WI}}s + 1}$$

which may be plotted as,

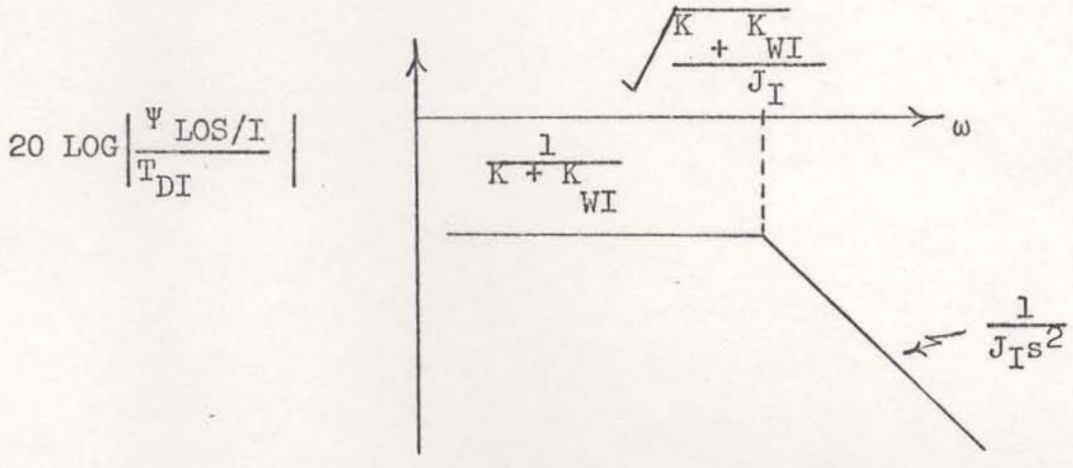

As seen from the sketch, low frequency disturbance rejection is provided primarily by the open loop gain (K) excluding the load since the gain is generally much larger than the gimbal compliance (K_{WI}) Without an integrator in the servo compensation, however, the low frequency disturbance rejection would be determined by just the gimbal compliance. At frequencies outside the loop bandwidth $\omega = \sqrt{\frac{K + K_{WI}}{J_I}}$, disturbance rejection is entirely dependent upon the gimbal inertia.

The low frequency gain term may be increased further by the addition of an integrating dipole to the servo compensation, i.e., $\frac{1 + s/\omega_1}{1 + s/\omega_2}$, where $\omega_2 < \omega_1$. The addition of this shaping requires that K be increased by ω_1/ω_2 which changes the low frequency response to:

$$\frac{\Psi_{LOS/I}}{T_{DI}} = \frac{\frac{1}{(\omega_1/\omega_2)K}\left(1 + s/\omega_2\right)}{(1 + s/\omega_1)} \; ; \; \omega < \sqrt{\frac{K + K_{WI}}{J_I}}$$

assuming $K_{WI} << K$.

The asymptotic frequency response is,

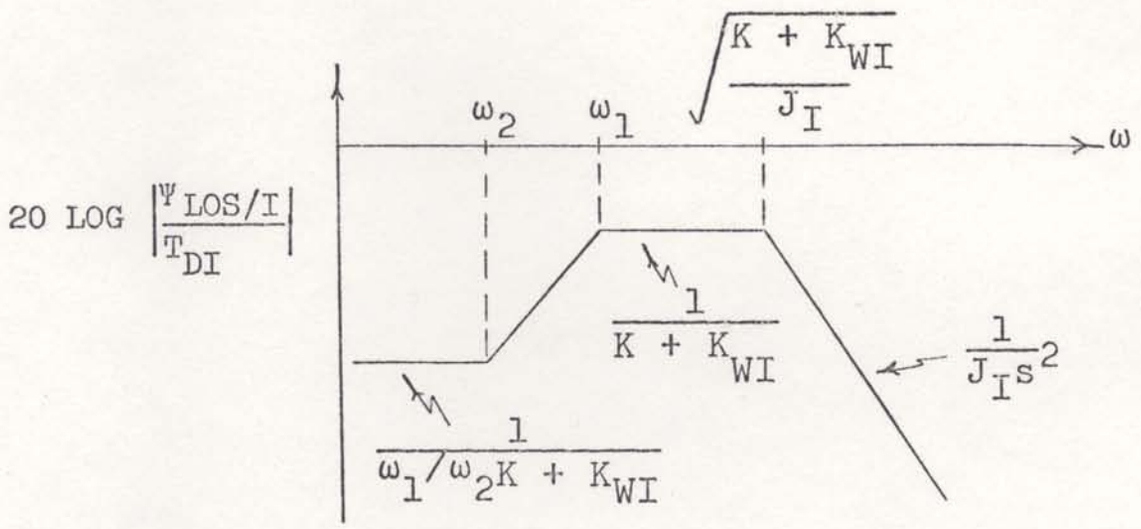

from which it may be seen that the low frequency disturbance rejection has been increased by the ratio ω_1/ω_2 just as the low frequency gain assuming K and thus $K(\omega_1/\omega_2) >> K_{WI}$.

After modifying the solution in equation (2), the ADR response of the yaw stabilized axis to outer gimbal yaw rates may be written as

$$\frac{\Psi_{LOS/I}}{\dot{\Psi}_{OG/I}} = \frac{\left(\frac{F_I}{K_{WI}} s + 1\right)}{s\left(\frac{J_I}{K_{WI}} s^2 + \frac{F_I + G_I(s)}{K_{WI}} s + 1\right)} \qquad (13)$$

which upon substituting $\frac{K\left(1 + s/\omega_n\right)}{s}$ for $G_I(s)$, is

$$\frac{\Psi_{LOS/I}}{\dot{\Psi}_{OG/I}} = \frac{\frac{K}{K + K_{WI}}\left(\frac{F_I}{K_{WI}} s + 1\right)}{s\left(\frac{J_I}{K + K_{WI}} s^2 + \frac{F_I + K/\omega_n}{K + K_{WI}} s + 1\right)}$$

and may be plotted as a function of frequency as,

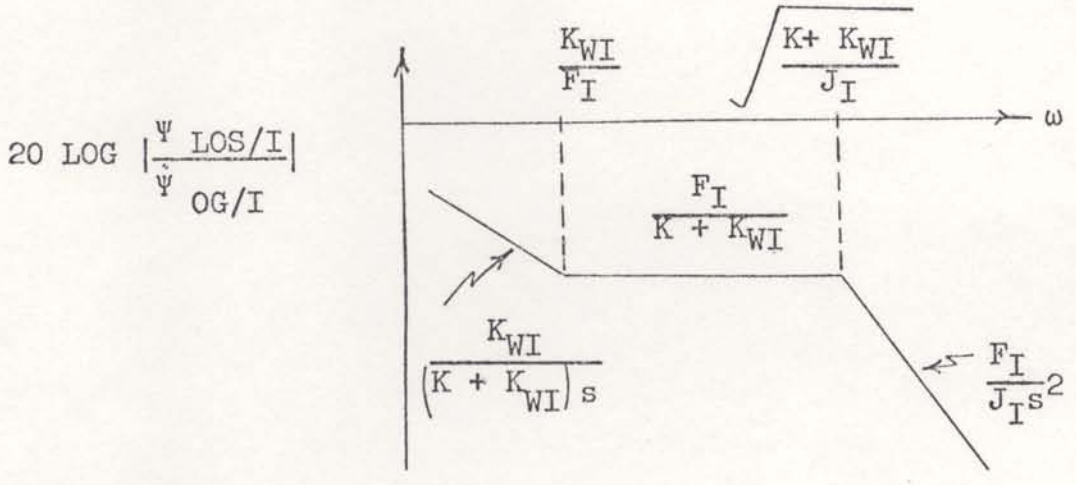

As shown in the plot of the yaw axis ADR response, the angular disturbance couples into LOS motion through the spring constant (K_{WI}) at low frequencies and through the gimbal friction (F_I) at higher frequencies as was the case with the momentum stabilized platform ADR (equations 6 and 7). The disturbance attenuation is determined by the open loop gain (K) excluding the load at frequencies within the

loop bandwidth $\sqrt{\frac{K + K_{WI}}{J_I}}$ and by the gimbal inertia at frequencies greater than the loop bandwidth.

With the addition of an integrating dipole $\frac{1 + s/\omega_1}{1 + s/\omega_2}$, where $\omega_2 < \omega_1$, the ADR becomes:

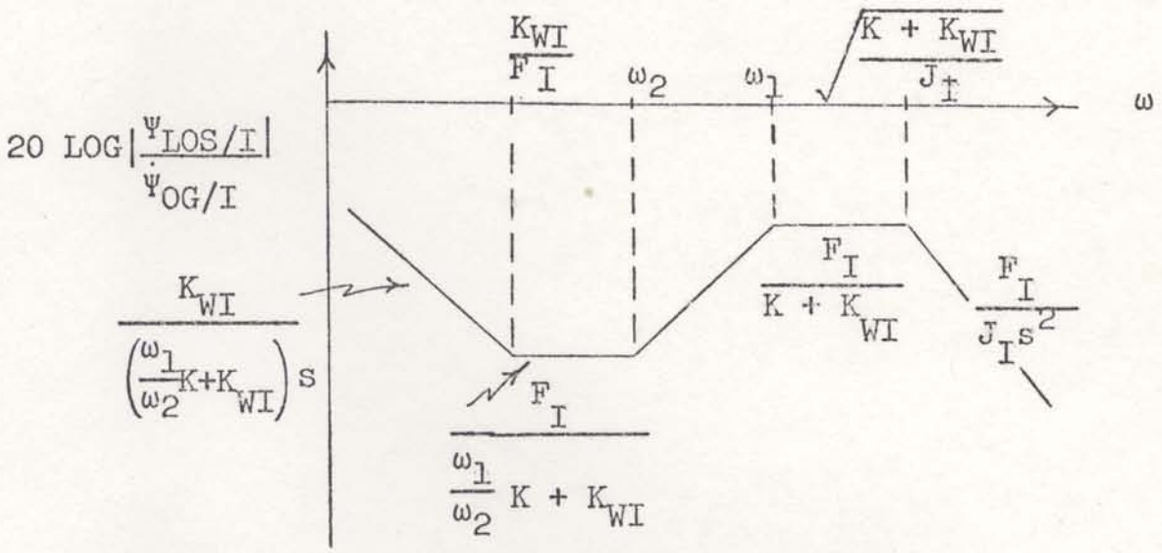

Here the dipole also increases the low frequency gain and thus the low frequency angular disturbance rejection capability.

Roll angular rates of the outer gimbal couple only into pitch motion of the LOS as may be observed from Figure 3 or the general solution. The ADR for the rate stabilized system to roll disturbance inputs may be derived from equation (2) as

$$\frac{\Theta_{LOS/I}}{\dot{\Phi}_{OG/I}} = \frac{\sin\Psi_{IG/OG}\left(\frac{J_O}{K_{WO}}s^2 + \frac{F_O}{K_{WO}}s + 1\right)}{s\left(\frac{J_O}{K_{WO}}s^2 + \frac{F_O + G_O(s)\cos\Psi_{IG/OG}}{K_{WO}}s + 1\right)} \qquad (14)$$

or letting $G_I(s) = K(1 + s/\omega_n)/s$ become,

$$\frac{\Theta_{LOS/I}}{\dot{\Phi}_{OG/I}} = \frac{\dfrac{K_{WO}\sin\Psi_{IG/OG}}{K_{WO} + K\cos\Psi_{IG/OG}}\left(\dfrac{J_O}{K_{WO}}s^2 + \dfrac{F_O}{K_{WO}}s + 1\right)}{s\left(\dfrac{J_O}{K_{WO} + K\cos\Psi_{IG/OG}}s^2 + \dfrac{(F_O + K/\omega_n)}{K_{WO} + K\cos\Psi_{IG/OG}}s + 1\right)}$$

which plots as shown below recognizing that $K >> K_{WO}$

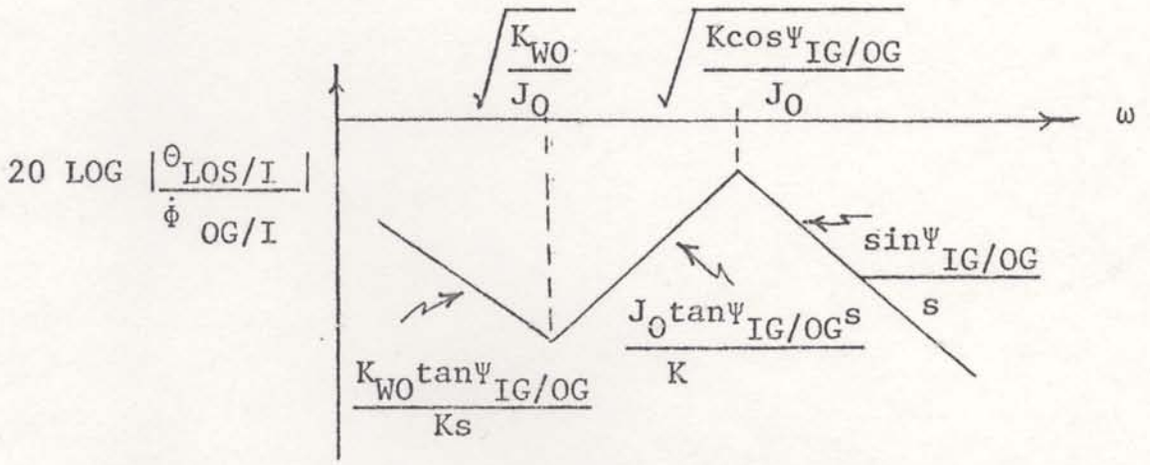

With the addition of vn integrating dipole, $\frac{(1 + s/\omega_1)}{(1 + s/\omega_2)}$ ($\omega_2 < \omega_1$), this ADR is,

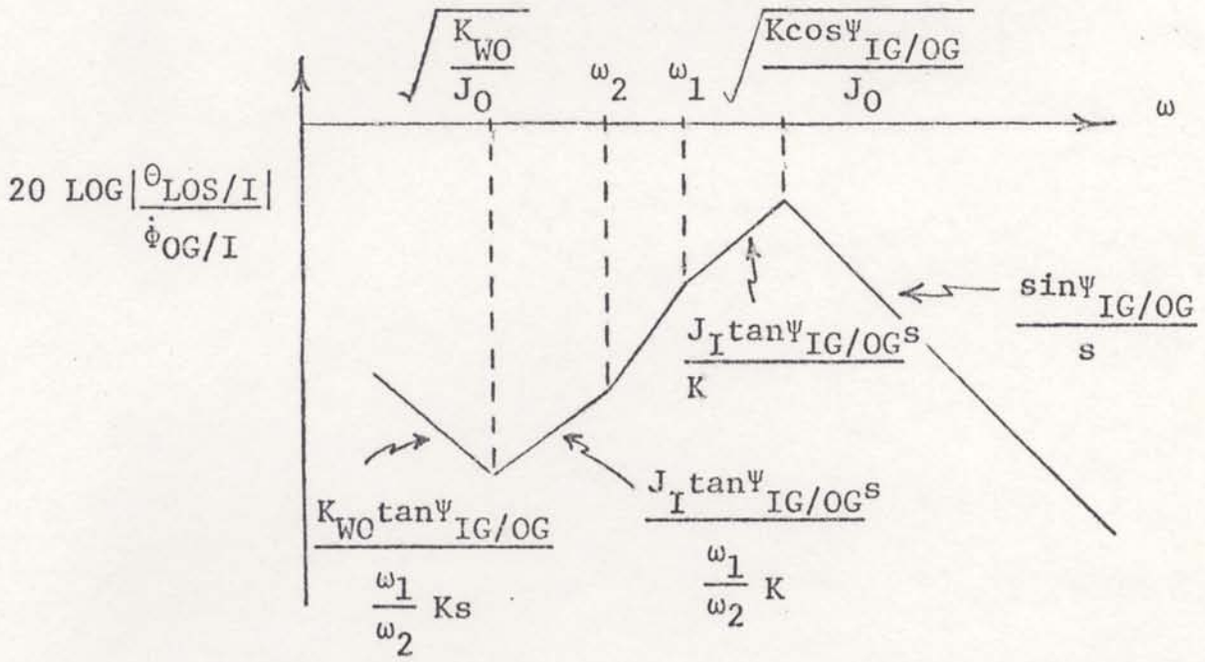

Both sketches show that below the loop bandwidth $\sqrt{\frac{K\cos\Psi_{IG/OG}}{J_O}}$ attenuation to roll disturbance inputs is provided by the electronic gain of the servo loop, either K or $\frac{\omega_1}{\omega_2}K$ depending on whether or not an integrating dipole is employed in the servo loop compensation. However, at frequencies greater than the loop bandwidth, roll disturbance rates couple into pitch LOS rate through the sine of the inner gimbal angle. There exists no inertia attenuation as in the cases of the inner gimbal mass unbalance disturbances and the pitch and yaw angular disturbances since the roll disturbance rate does not enter about a stabilized axis. This is also true for the pitch axis response to roll inputs in a momentum stabilized system, equation (9).

2.5 Secondary Disturbance Sources and Primary Nonlinearities

The analysis thus far has derived the disturbance models for the environmental inputs which are the primary sources of stabilization error. For completeness, the secondary disturbance sources will be mentioned herein. The system nonlinearities, however, may have a significant impact upon the models which have been developed and a technique for evaluating these effects will also be presented.

The principal secondary disturbance sources are gyro noise in rate stabilized systems and magnetically induced

torques in momentum stabilized systems [2]. Since the predominant components of gyro noise occur at high frequencies relative to the system bandwidth [3], the noise induced LOS motion is not usually high. However, there can be a significant effect on the torque motor form factor in terms of excessive heating. Gyro noise effects may be predicted with the same techniques applied previously to derive the environmental disturbance models. Momentum stabilized platforms respond to magnetically induced torques with a low frequency drift rate which is not of primary concern here.

The most significant nonlinearity is coulomb friction which impacts both stabilization concepts. Coulomb friction is defined as a constant retarding torque independent of the relative gimbal rate as opposed to viscous friction which is directly proportional to the relative gimbal rate. Since coulomb friction is the predominant friction present, and as noted earlier, the angular vibration environment couples into LOS motion through the gimbal friction and spring constant, it is necessary to include this nonlinearity in the disturbance models.

Coulomb friction is generally represented with a bang-bang function, i.e.,

$$T_F = F_C \mathrm{sgn}(\dot{\Psi}_{IG/OG})$$

where T_F = friction torque

F_C = friction amplitude

For some environments, the coulomb friction effect may be adequately linearized to allow use of linear disturbance models. Considering a line spectra disturbance with a single frequency predominating, the output of the coulomb friction model will be a square wave of the same frequency as the input. This square wave may be treated as a torque disturbance input and may be approximated sinusoidally by the first term of its Fourier expansion as:

$$T_F = (4F_C/\pi) \sin (2\pi f_c t)$$

where f_c is the predominant frequency of the input environment ($\dot{\Psi}_{OG/I}$)[4]. The frequency of the input environment is used as opposed to the relative gimbal rate ($\dot{\Psi}_{IG/OG}$) frequency since the gimbal inertial rate ($\dot{\Psi}_{IG/I}$) should be small in comparison to the input environment if the system is stabilized. This approximation may now be used in conjunction with the TDR ratio as described in the next section.

2.6 Performance Determination

Determining the environmentally induced LOS jitter basically entails combining the input environment with the appropriate disturbance rejection response. The manner in which this is done depends on the input environment spectral type.

1. Continuous Spectra -- If the input environment is represented with a continuous (random) spectra, the amount of LOS motion may be calculated by,

$$\varepsilon_i = \int_0^\infty |DRR(f)|^2 D(f)df \qquad (15)$$

where ε_i = Stabilization Error

DRR(f) = The disturbance rejection ratio for D(f)

D(f) = Input environment power spectral density

Then the total stabilization error is the root sum square total of the errors created from each disturbance input, i.e.,

$$\varepsilon_T = \left(\sum_{i=1}^{n} \varepsilon_i^2\right)^{\frac{1}{2}}$$

2. Line Spectra -- If the input environment is represented with a line spectra, i.e., a finite sum of sinusoids, the LOS motion may be calculated from

$$\varepsilon_i = \left(\sum_{j=1}^{k} [D(f_j)DDR(f_j)]^2\right)^{\frac{1}{2}} \qquad (16)$$

where ε_i = Stabilization Error

$D(f_j)$ = Input environment at frequency f_j

$DDR(f_j)$ = The disturbance rejection ratio at frequency f_j

and the total LOS error is also

$$\varepsilon_T = \left(\sum_{i=1}^{n} \varepsilon_i^2\right)^{\frac{1}{2}}$$

This assumes that the line spectra is phase independent.

3.0 CASE STUDY

3.1 System Definition

To demonstrate the disturbance models and coulomb friction approximation presented in Section 2, representative momentum and rate stabilization systems were chosen for analysis. Both systems have been designed for deployment as seekers on the same missile and thus have the same form factor and requirements. These momentum and rate stabilized platforms are presented in block diagram form in Figures 4 and 5. Only the inner gimbal is represented for the rate stabilized platform since there is no cross-coupling effects to consider in the rate stabilized model and the outer gimbal follows the same relationship as the inner gimbal.

3.2 Model Verification

The actual disturbance rejection responses have been calculated based on the linear models of Figures 4 and 5 using a block diagram reduction program, ACAP (Automatic Control Analysis Program)[5] which is available on the Martin Marietta Aerospace computer system. ACAP takes input in the form of a block diagram, reduces the block diagram and calculates the roots and indicated frequency responses.

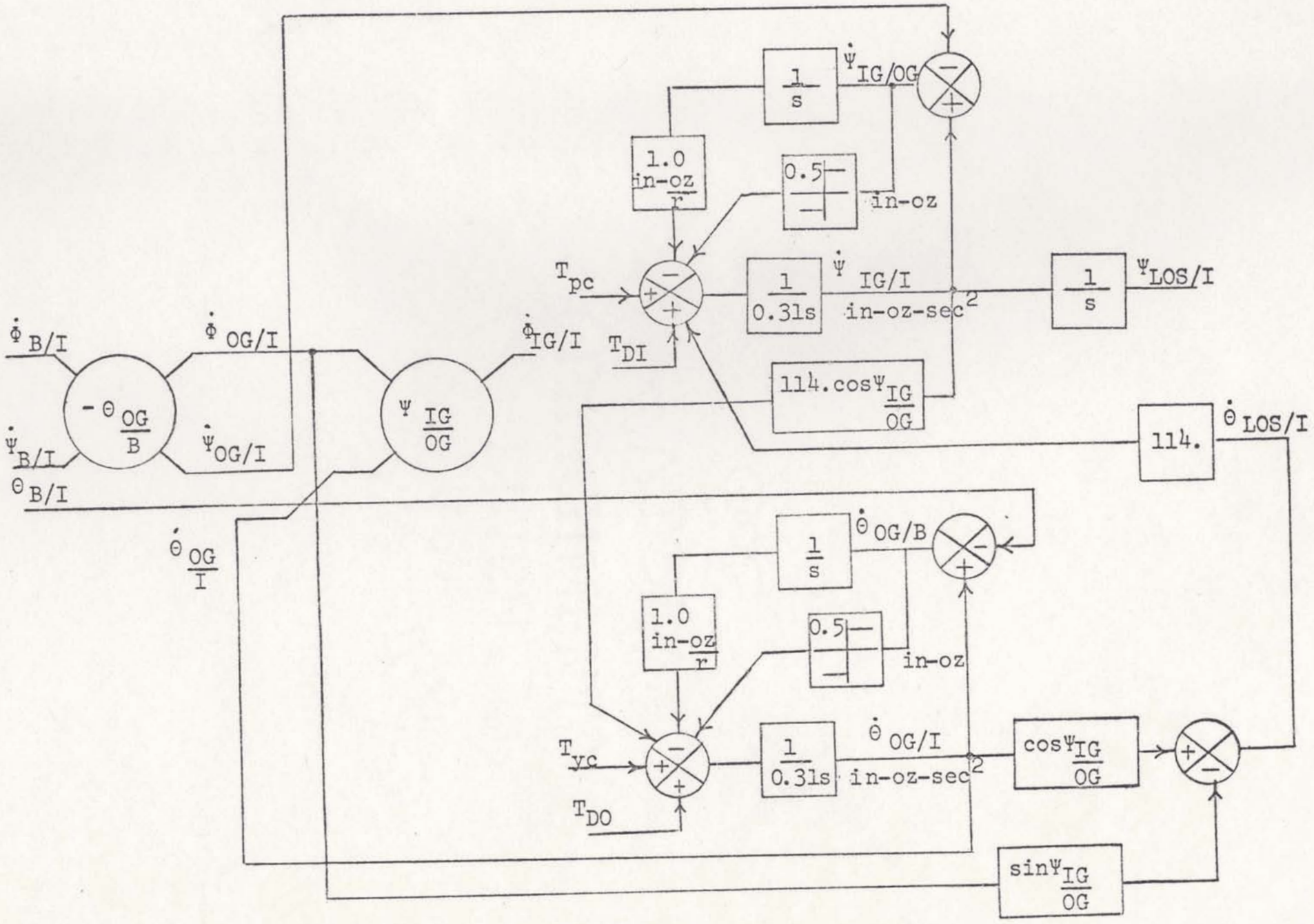

Figure 4. Momentum System Case Study Block Diagram

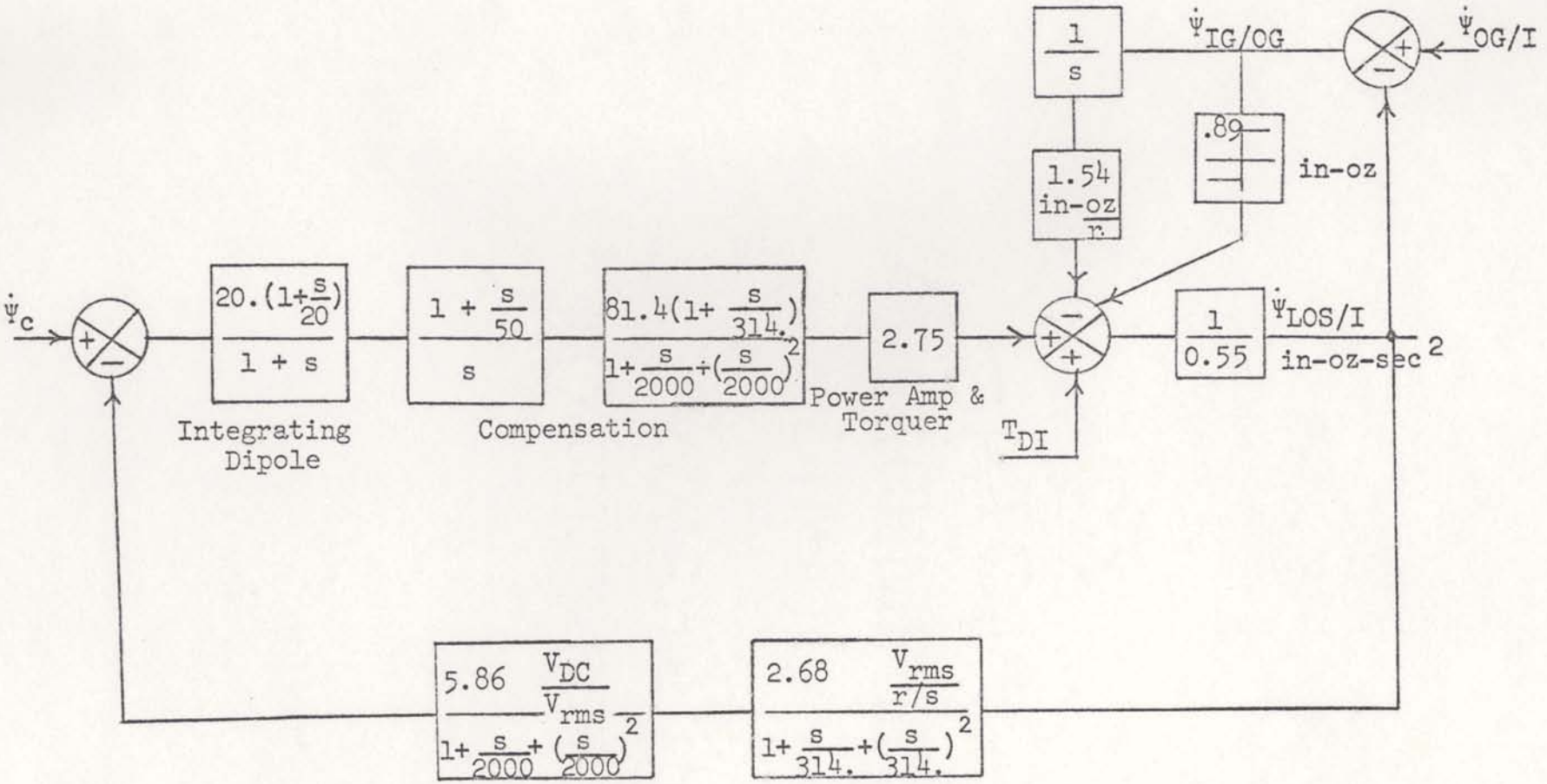

Figure 5. Rate System Case Study Block Diagram

Figures 6 - 10 present all the disturbance rejection responses of the yaw (LOS) axis for a momentum stabilized system. This includes the TDR responses for both inner and outer gimbal mass unbalance torques and the ADR responses for outer gimbal yaw, body pitch, and body roll rates. The asymptotes plotted with these curves were calculated from approximations used in the disturbance models of Section 2.3. The model derived asymptotes show almost exact agreement with the computer calculated frequency responses.

Figures 11 and 12 present all the disturbance rejection responses associated with the yaw LOS axis for a rate stabilized system. These are the TDR response to inner gimbal mass unbalance torques and the ADR response to outer gimbal roll rates. These responses also have the asymptotes plotted, based on the disturbance rejection models in Section 2.4. The asymptotes agree with the calculated responses except for $200 < \omega < 500$ rad/sec. where the rate gyro and higher frequency poles enter but the difference is not great ($\sim$5 db).

To evaluate the validity of the coulomb friction approximation made in Section 2.5, a nonlinear simulation of the rate stabilized platform was programmed, based on the block diagram of Figure 5. A 10 Hz outer gimbal yaw motion was the disturbance input and the resulting yaw LOS motion is plotted in Figure 13. The results show a yaw LOS motion of 0.184 milliradian zero-to-peak. Using the approximation

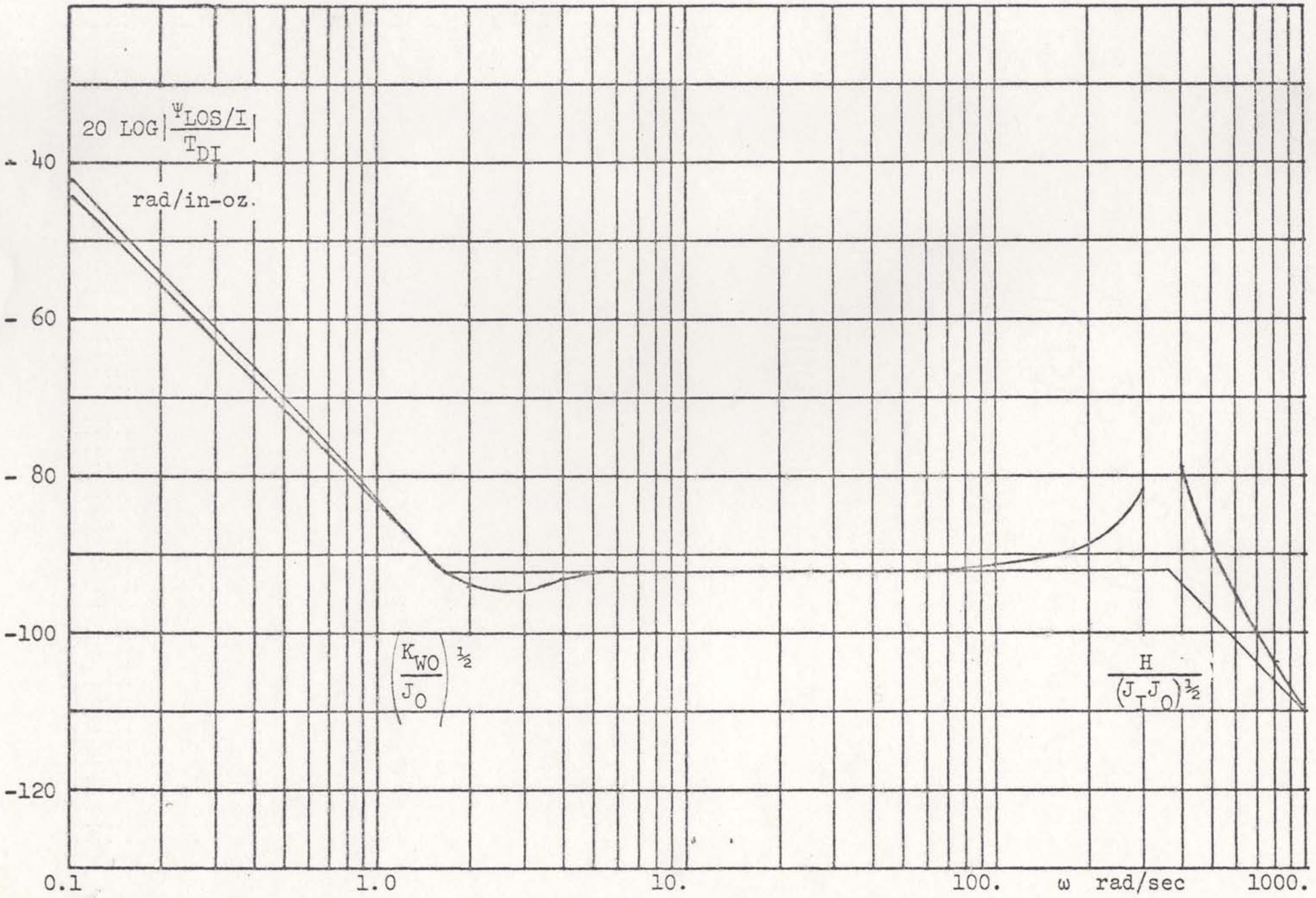

Figure 6. Momentum Stabilization Yaw TDR Response to Inner Gimbal Mass Unbalance Torques

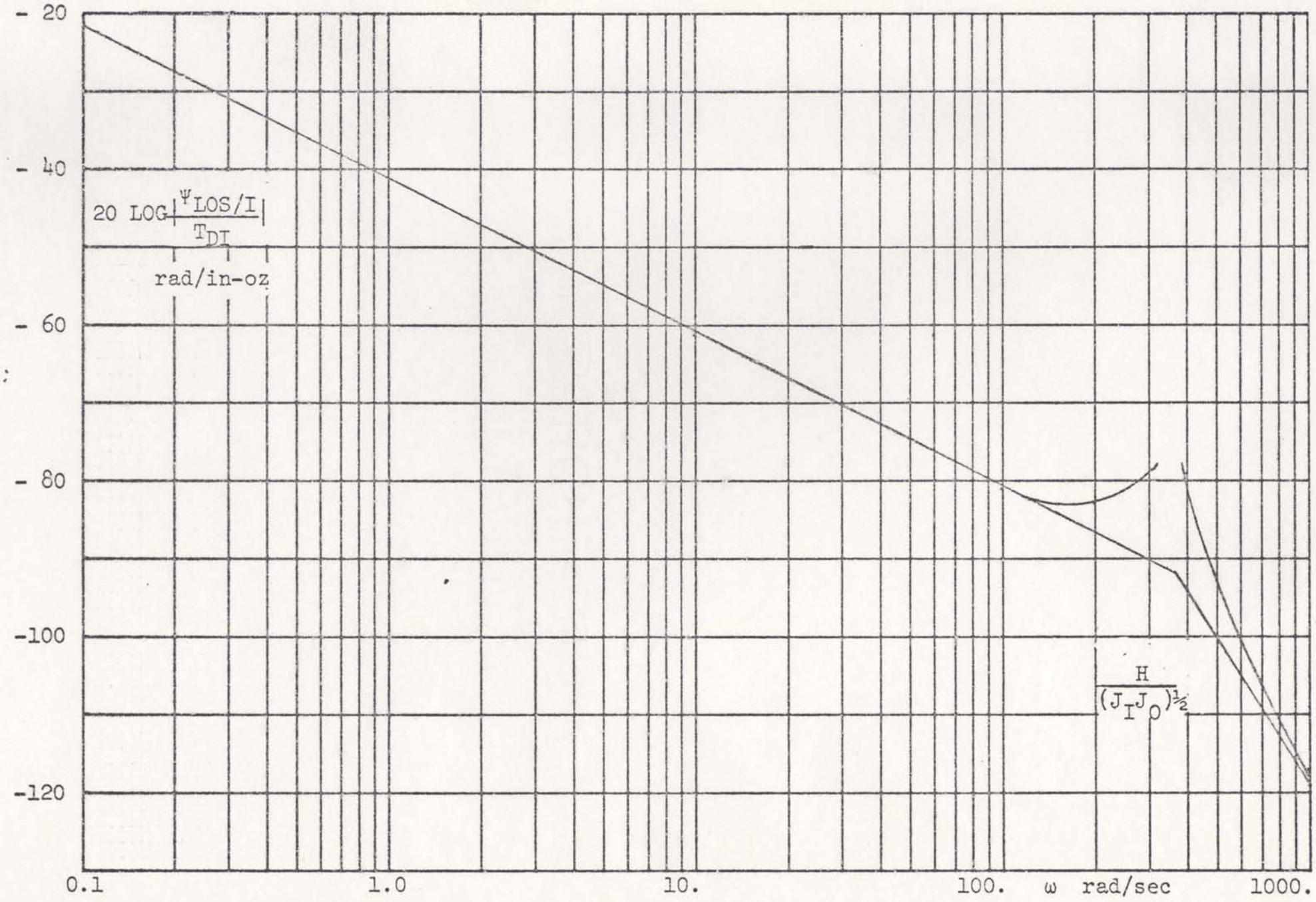

Figure 7. Momentum Stabilization Yaw TDR Response To Outer Gimbal Mass Unbalance Torques

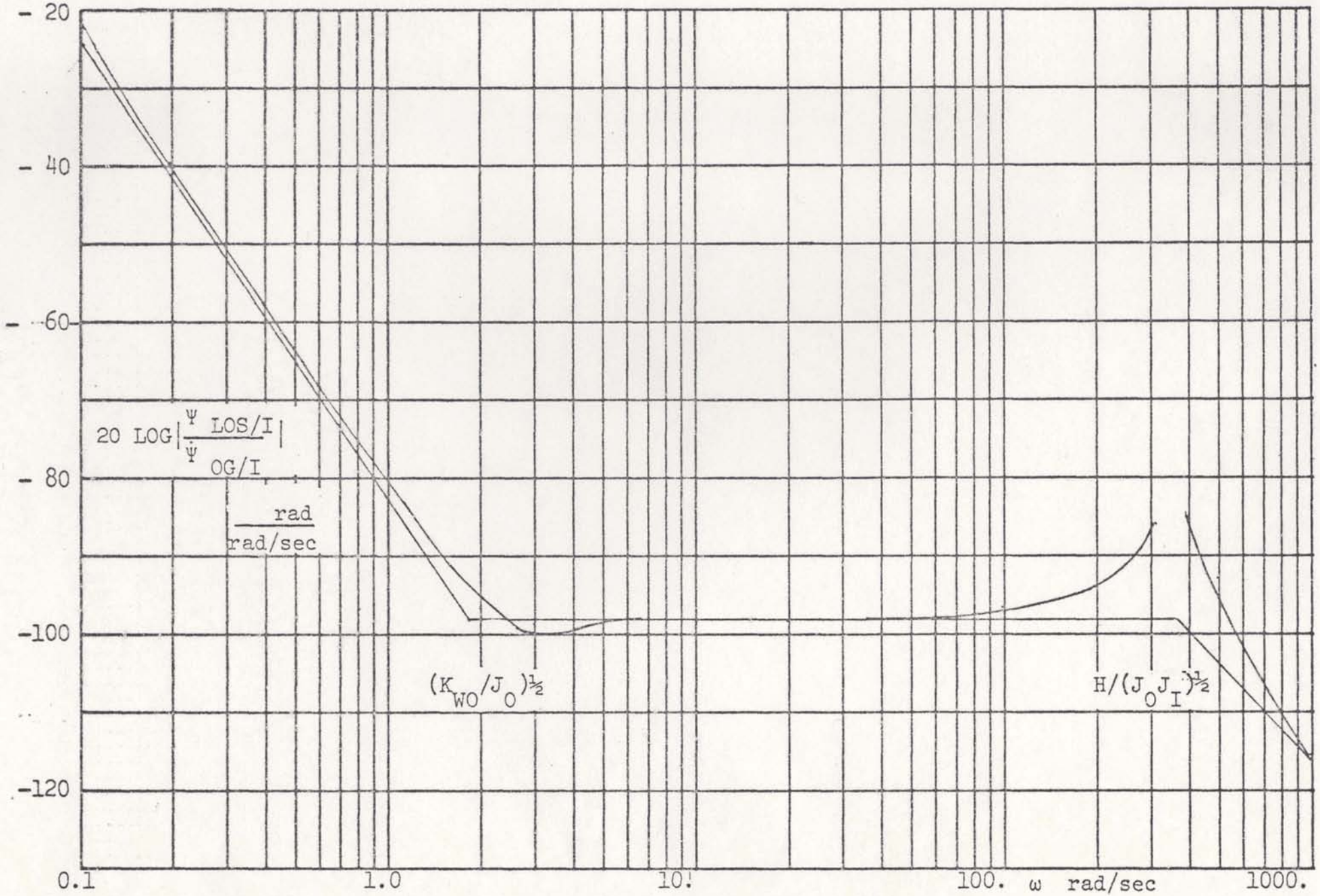

Figure 8. Momentum Stabilization Yaw ADR Response To Outer Gimbal Yaw Rates

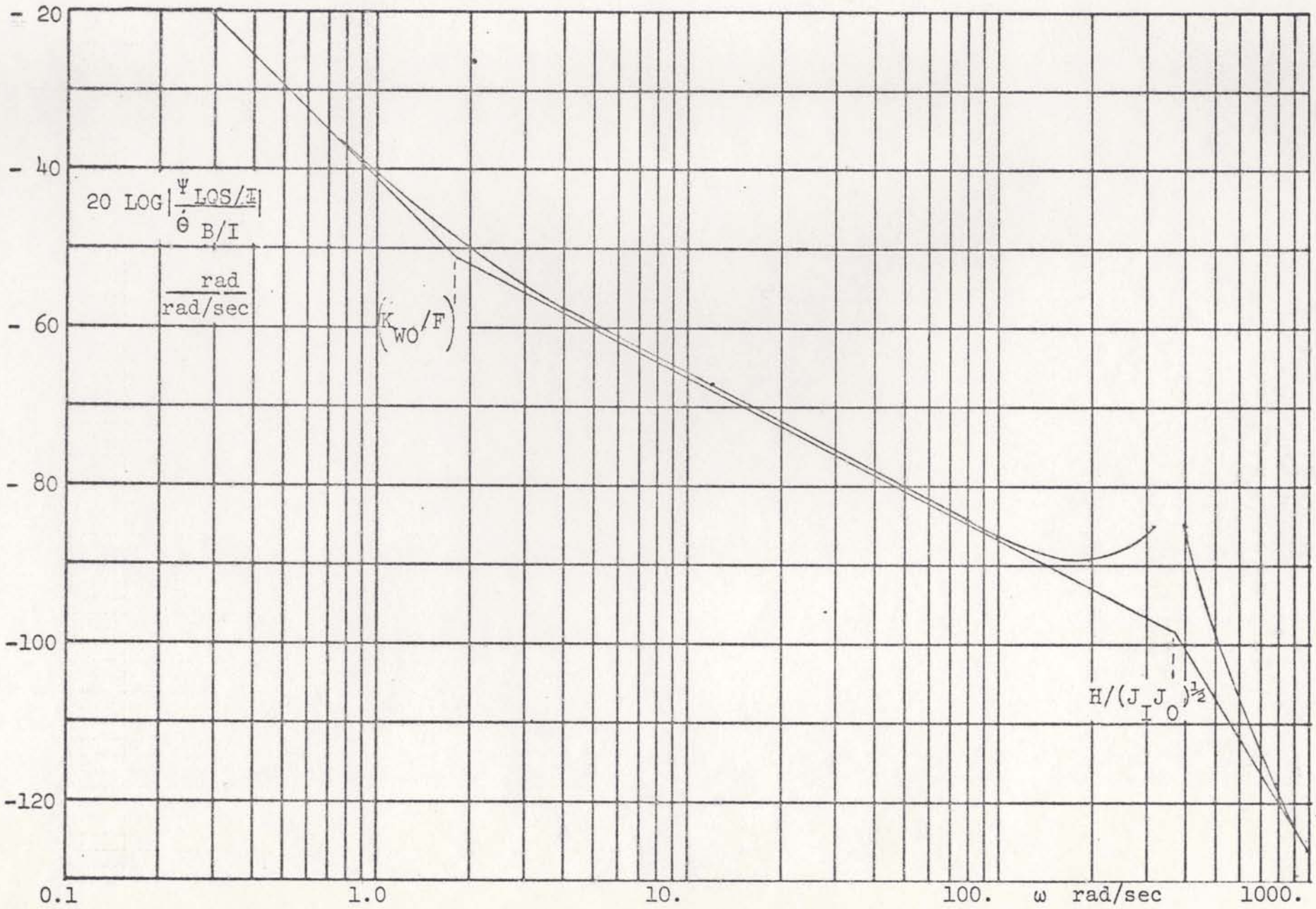

Figure 9. Momentum Stabilization Yaw ADR Response To Body Pitch Rates

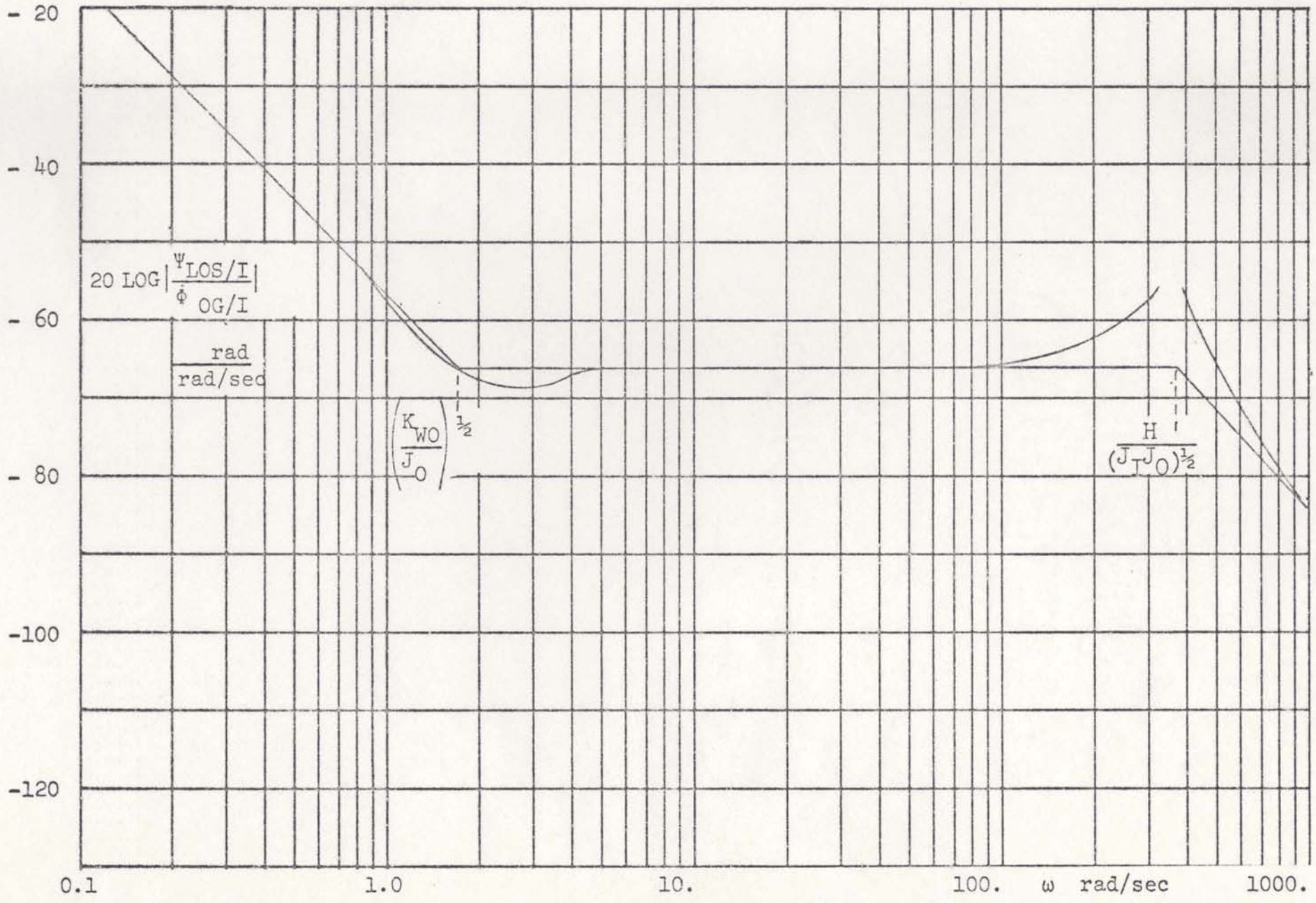

Figure 10. Momentum Stabilization Yaw ADR Response To Outer Gimbal Roll Rates

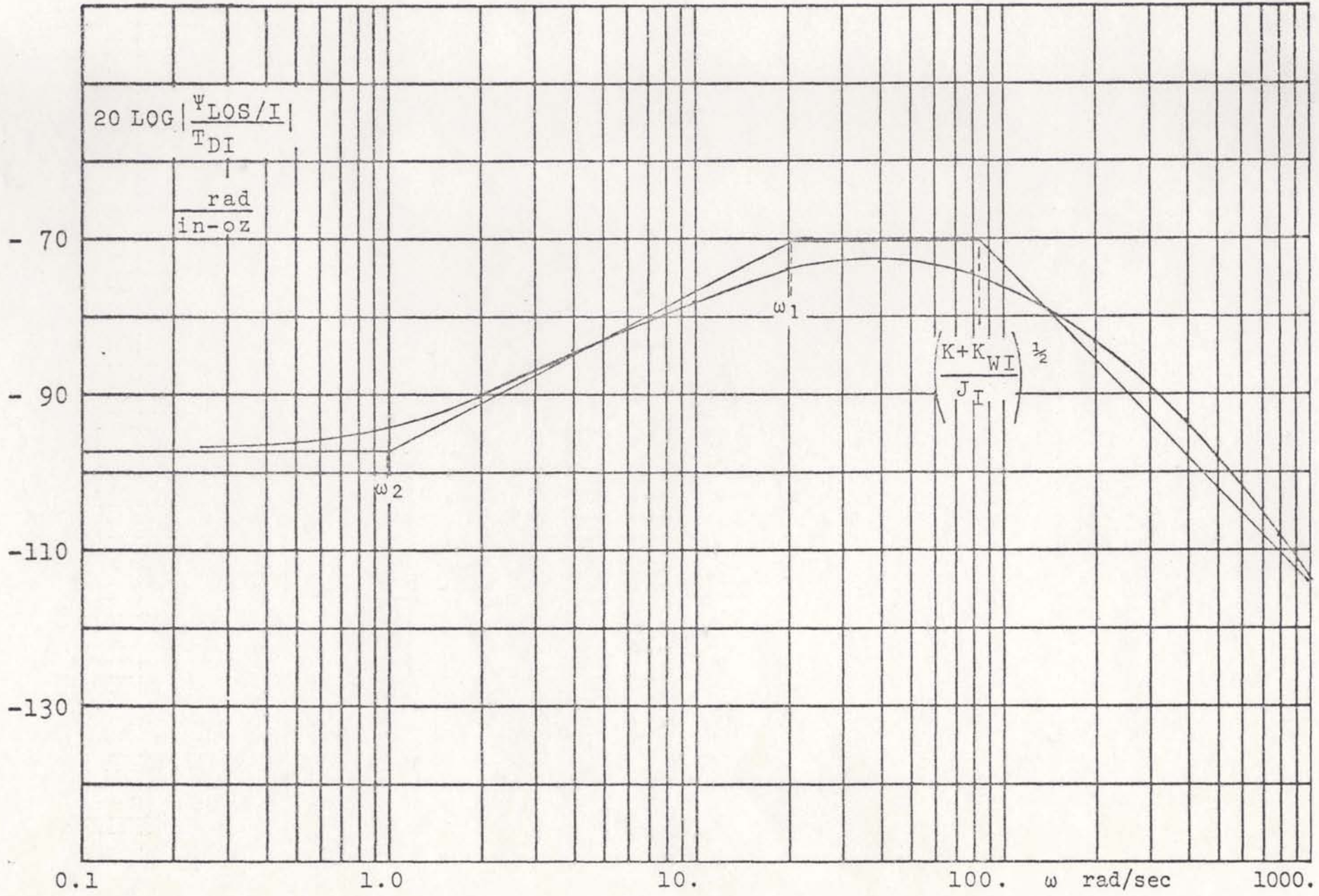

Figure 11. Rate Stabilization Yaw TDR Response To Yaw Mass Unbalance Torque

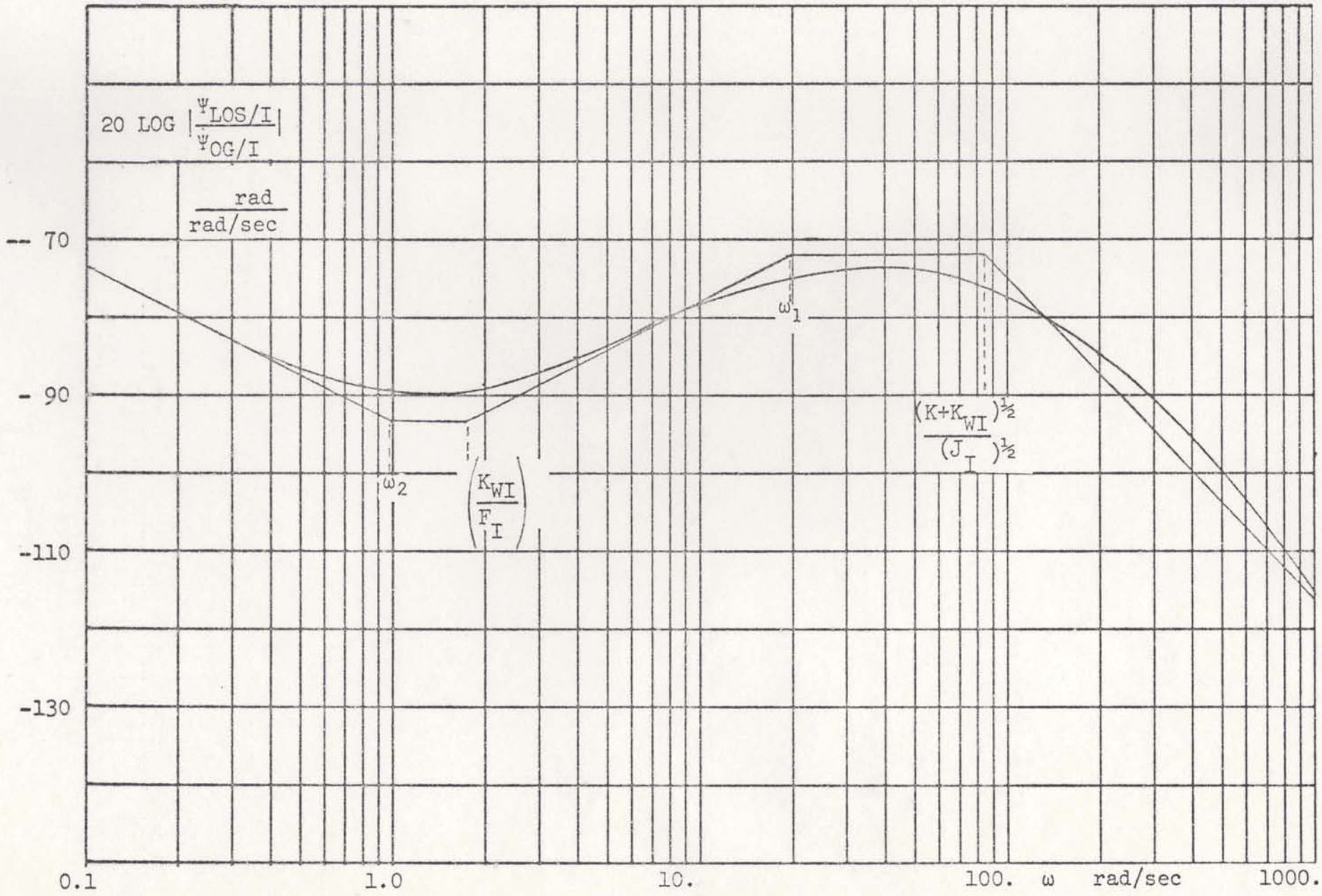

Figure 12. Rate Stabilization Yaw ADR Response To Outer Gimbal Yaw Rates

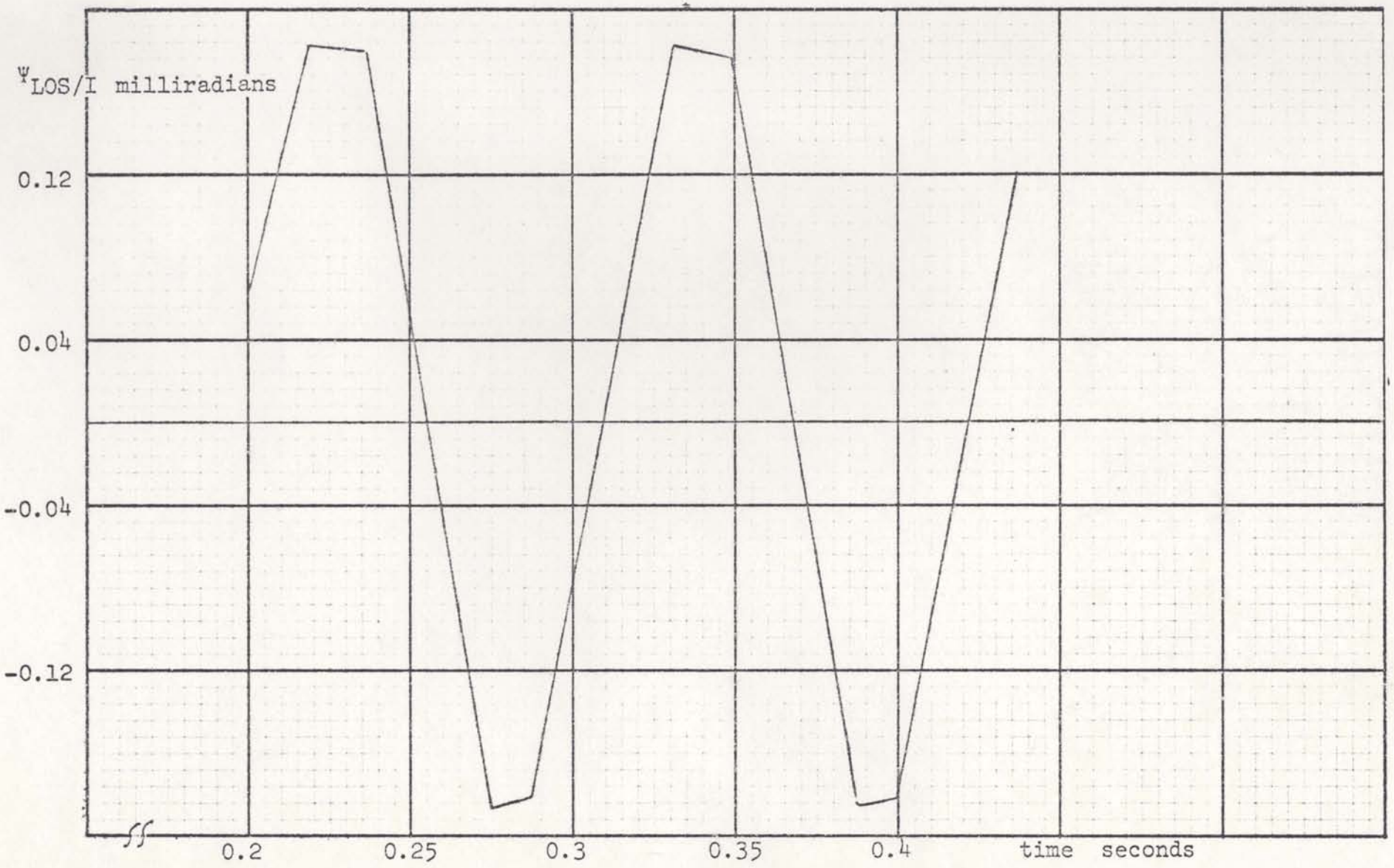

Figure 13. Nonlinear Simulation Results

of Section 2.5 and Figure 11, the yaw gimbal TDR response, the approximated value is 0.226 milliradian of motion. The approximation then is somewhat conservative, being 23 per cent higher than the value arrived at by simulation. The approximation is valid enough to be useful considering it does not require a nonlinear simulation.

3.3 Stabilization Performance

To compare the performance of the two stabilization systems, a simplified helicopter environment will be assumed. This is a line spectra environment consisting of a linear vibration environment of 2.g's zero-to-peak at 11, 22, and 33 Hz and roll, pitch, and yaw angular vibration environments of 2.0 milliradians/sec. zero-to-peak at 11 Hz. The gimbals are all assumed to be balanced to .05 in-oz/g and the coulomb and viscous (linear) friction terms are assumed to be equal.

Since this is a line spectra environment, equation (16) applies. Using this equation with the above environment and the disturbance rejection responses of Section 3.2, the stabilization accuracy has been calculated for both systems and is presented in TABLE 1.

The momentum stabilized platform has the lower LOS motion by a factor of 2.7 over the rate stabilized system. It should be noted from the disturbance rejection curves that this result is dependent upon the frequency content of the environment. A lower frequency environment would cause the

opposite to be true.

TABLE 1 also shows that coulomb friction is the largest contributor to LOS motion. Even assuming equal coulomb and viscous friction components, the coulomb friction effect was still two orders of magnitude greater than that of the viscous friction. The difference in coulomb friction between the two stabilization examples also accounts for most of the difference in stabilization performance of the two systems. If the coulomb frictions were equal, the momentum stabilized platform would provide less LOS motion in this environment by a factor of 1.5 over the rate stabilized system instead of 2.7.

TABLE 1 --Inner Gimbal Stabilization Accuracy

Disturbance Source	Yaw LOS Motion	
	Momentum System	Rate System
Inner Gimbal Mass Unbalance Torques	2.8 μrad	11.6 μrad
Outer Gimbal Mass Unbalance Torques	8.04 μrad	. . . . .
Yaw Outer Gimbal Rates	.063 μrad	0.53 μrad
Pitch Body Rates	0.134 μrad	. . . . .
Roll Body Rates	1.0 μrad	. . . . .
Inner Gimbal Coulomb Friction	15.7 μrad	226. μrad
Outer Gimbal Coulomb Friction	82.0 μrad	. . . . .
RSS Total	85.2 μrad	226.3 μrad

4.0 SUMMARY AND CONCLUSIONS

An environmental disturbance model has been derived for the general stabilization case which applies directly to momentum stabilized platforms. From this general model, the rate stabilized platform solution was also derived. The linear disturbance rejection models were presented in detail for each disturbance input and explicitly identified the contribution of the various system parameters to disturbance rejection. This detailed presentation also provided asymptotic approximations which allow the system performance to be initially evaluated without a detailed simulation. A method for predicting stabilization performance based on these disturbance models was introduced and appropriately modified to include the significant system nonlinearities.

To demonstrate these techniques and the validity of the model derived asymptotic approximations, a case study was conducted on equivalent momentum and rate stabilized systems. The disturbance models were shown to be accurate representations by evaluating the original system equations with the aid of a computer block diagram reduction program. A nonlinear simulation of the rate stabilized platform was programmed and confirmed that the linear

approximation of the most significant nonlinearity, coulomb friction, to be accurate within 23 percent. Using a simplified helicopter environment to compare the rate and momentum stabilized platform performance showed the systems to be nearly equal within a factor of 2.7 in overall LOS motion. As noted in the text, stabilization performance is strongly a function of the frequency content of the environment.

In general, the momentum system stabilized systems rejection is inversely proportional to a function of the angular momentum of its spinning mass at frequencies less than the system natural frequency. For disturbances coupling directly into the inner gimbal, and hence the LOS, the rejection capability is inversely proportional to the square of the angular momentum. For disturbances coupling from the outer gimbal into the inner indirectly through the momentum, the disturbance rejection is inversely proportional to the momentum. At frequencies higher than the system natural frequency, disturbance attenuation is determined solely by the system inertias except in the case of a roll disturbance input.

The rate stabilized system disturbance rejection capability is determined primarily by the open servo loop gain excluding the load. At frequencies within the system bandwidth, the disturbance rejection response is inversely proportional to the gain. At higher frequencies, all the

disturbance rejection, except for the roll disturbance inputs, is provided by the gimbal inertia. The low frequency electronic gain may be increased through the utilization of appropriate shaping networks as was shown in Section 2.4. However, once the loop bandwidth is fixed, which is usually done by the selection of the rate sensor, it can be easily shown from the open loop frequency response that the achievable electronic loop gain is a direct function of gimbal inertia. Therefore, any overall improvement in disturbance rejection response at all frequencies requires an increase in inertia. Neither stabilization system provides any rejection of roll rates entering the outer gimbal at frequencies greater than the system natural frequency. Since this disturbance occurs about an unstabilized axis, there is no attenuation provided by the gimbal inertia.

The models presented in this paper yield both an understanding of momentum and rate stabilized platforms and the techniques necessary to determine stabilization performance. The relationships of the gimbal parameters and electronic compensation to stabilization performance that were drawn from the models provide a useful design tool in the early stages of mechanical and electrical trade off studies. Since the models were also shown to be adaptable to the inclusion of the significant nonlinearities, they may also be employed to analyze performance saving the cost

and time required to implement detailed computer simulations.

5.0 APPENDIX

5.1 Momentum Stabilization Dynamic Equation Derivation

The dynamic equations for the 2-DOF momentum stabilized platform may be derived from Newton's second law for angular motion [6], which states that the sum of the external torques (ΣT_{EXT}) acting upon a body is equal to the time rate of change of its angular momentum, i.e.,

$$\Sigma T_{EXT} = \frac{d\bar{H}}{dt} = \frac{\partial \bar{H}}{\partial t} + \bar{\omega} \times \bar{H}$$

where $\bar{H}$ = total angular momentum

$d\bar{H}/dt$ = time derivative of H with respect to the inertial frame

$\partial\bar{H}/\partial t$ = time derivative of H with respect to the moving frame

$\bar{\omega}$ = inertial angular velocity of moving frame

Assuming that the inner and outer gimbal principle axes are aligned with their respective coordinate frames which are identified here with subscripts I and O, the inner gimbal angular momentum can be expressed as,

$$H_I = (J_{IX}\dot{\Phi}_{IG/I} + H_s)\hat{i}_I + J_{IY}\dot{\Theta}_{IG/I}\hat{j}_I + J_{IZ}\dot{\Psi}_{IG/I}\hat{k}_I$$

where H_s is the spinning wheel angular momentum, and J_{IX},

J_{IY}, and J_{IZ} are the inner gimbal moments of inertia. The inertial angular velocity of the inner gimbal is expressed as,

$$\bar{\omega}_I = \dot{\Phi}_{IG/I}\hat{i}_I + \dot{\Theta}_{IG/I}\hat{j}_I \quad \dot{\Psi}_{IG/I}\hat{k}_I$$

Similarly, the outer gimbal angular momentum may be expressed as,

$$\bar{H}_O = J_{OX}\dot{\Phi}_{OG/I}\hat{i}_O + J_{OY}\dot{\Theta}_{OG/I}\hat{j}_O + J_{OZ}\dot{\Psi}_{OG/I}\hat{k}_O$$

with $$\bar{\omega}_O = \dot{\Phi}_{OG/I}\hat{i}_O + \dot{\Theta}_{OG/I}\hat{j}_O + \dot{\Psi}_{OG/I}\hat{k}_O$$

Noting from Figure 1, the following relationships apply,

$$\hat{i}_I \cdot \hat{j}_O = \sin\Psi_{IG/OG}$$
$$\hat{j}_I \cdot \hat{j}_O = \cos\Psi_{IG/OG}$$
$$\hat{k}_I \cdot \hat{j}_O = 0$$

The two torque equations may be written as,

$$\Sigma T_{IZ} = J_{IZ}\ddot{\Psi}_{IG/I} + (J_{IY} - J_{IX})\dot{\Phi}_{IG/I}\dot{\Theta}_{IG/I} - H_s\dot{\Theta}_{IG/I}$$

$$\Sigma T_{OY} = J_{OY}\ddot{\Theta}_{OG/I} + (J_{OX} - J_{OZ})\dot{\Phi}_{OG/I}\dot{\Psi}_{OG/I} +$$

$$\sin\Psi_{IG/OG}\left(J_{IX}\ddot{\Phi}_{IG/I} + (J_{IZ} - J_{IY})\dot{\Theta}_{IG/I}\dot{\Psi}_{IG/I}\right) +$$

$$\cos\Psi_{IG/OG}\left(J_{IY}\ddot{\Theta}_{IG/I} + (J_{IX} - J_{IZ})\dot{\Phi}_{IG/I}\dot{\Psi}_{IG/I} + H_s\dot{\Psi}_{IG/I}\right)$$

which using the following transformations,

$$\ddot{\Phi}_{IG/I} = \ddot{\Phi}_{OG/I}\cos\Psi_{IG/OG} + \ddot{\Theta}_{OG/I}\sin\Psi_{IG/OG}$$

$$\ddot{\Theta}_{IG/I} = -\ddot{\Phi}_{OG/I}\sin\Psi_{IG/OG} + \ddot{\Theta}_{OG/I}\cos\Psi_{IG/OG}$$

and assuming that the product terms such as $\dot{\Theta}_{IG/I}\dot{\Psi}_{IG/I}$ and the quantity $(J_{IX} - J_{IY})$ are negligible, the above expressions simplify to:

$$\Sigma T_{IZ} = J_{IZ}\ddot{\Psi}_{IG/I} - H_s\dot{\Theta}_{IG/I}$$

$$\Sigma T_{OY} = J_{OY}\ddot{\Theta}_{IG/I} + H_s \cos\Psi_{IG/OG}\dot{\Psi}_{IG/I}$$

These are the basic equations of motion for a 2-DOF stabilized platform. To these equations, can be added the external disturbance torques coupling through gimbal mass unbalance, friction, and compliance.

6.0 LITERATURE CITED

1. Rue, A.K. "Precision Stabilization Systems." IEEE Transactions Aerospace and Electronic Systems AES 10 (January 1974): 34-42.

2. White, S.A. "Dynamics of a Solenoidal-Torqued Gyro Stabilized Seeker Assembly for Guidance and Tracking Systems." IEEE Transactions Aerospace and Electronic Systems AES 10 (January 1974): 113-22.

3. Sieb, L. E. "DTTS Rate Integrating Gyro Test." Martin Marietta Aerospace Orlando Report AAO ANA 70801000-001, January 1974.

4. Gregg, J. E. "A Method For Predicting Servo Ripple Due to Stick-Slip Friction." Electromechanical Design, March 1973, 24-27.

5. "Automatic Control Analysis Program." Martin Marietta Aerospace Orlando Utilization Report Q005, January 1969.

6. Winsor, C. A. "Two-DOF Gyro Model." Martin Marietta Aerospace Orlando Report AAO ANA 70801000-001, January 1974.